1-1-2014

A bounding surface plasticity model for highly crushable granular materials

Mojtaba E. Kan
University of New South Wales, mojtaba@uow.edu.au

Hossein Taiebat
University of New South Wales, h.taiebat@unsw.edu.au

A bounding surface plasticity model for highly crushable granular materials

Abstract

A bounding surface plasticity model is presented for crushable rockfills in the framework of the critical state soil mechanics which includes translation of the critical state line due to particle crushing. A translating limiting isotropic compression line is also introduced and incorporated in the model to describe the position and evolution of the bounding surface. A particle breakage index is introduced as a function of stress invariants which controls the translation of the critical state and limiting isotropic compression lines. The performance of the model is demonstrated using the results of experimental tests on different types of rockfill materials conducted under both monotonic and cyclic loading conditions. The study shows the capability of the model in capturing the characteristic features of the behavior of rockfill and other crushable materials such as ballast and coarse gravel under both conventional and complex loading paths.

Publication Details

Kan, M. E. & Taiebat, H. A. (2014). A bounding surface plasticity model for highly crushable granular materials. Soils and Foundations, 54 (6), 1188-1201.

A Bounding Surface Plasticity Model for Highly Crushable Granular Materials

Mojtaba E. Kan[1] and Hossein A. Taiebat[2]

Abstract: A bounding surface plasticity model is presented for crushable rockfills in the framework of the critical state soil mechanics which includes translation of the critical state line due to particle crushing. A translating limiting isotropic compression line is also introduced and incorporated in the model to describe the position and evolution of the bounding surface. A particle breakage index is introduced as a function of stress invariants which controls the translation of the critical state and limiting isotropic compression lines. The performance of the model is demonstrated using the results of experimental tests on different types of rockfill materials conducted under both monotonic and cyclic loading conditions. The study shows the capability of the model in capturing the characteristic features of the behaviour of rockfill and other crushable materials such as ballast and coarse gravel under both conventional and complex loading paths.

Keywords: rockfill; bounding surface plasticity; particle breakage; cyclic loading

[1] PhD Candidate, School of Civil and Environmental Engineering, The University of New South Wales, Sydney, NSW 2052, Australia. Email: m.esfahanikan@unsw.edu.au

[2] Senior Lecturer, School of Civil and Environmental Engineering, The University of New South Wales, Sydney, NSW 2052, Australia. Email: h.taiebat@unsw.edu.au (Corresponding author)

1. INTRODUCTION

Rockfills are widely used in earth and rockfill dams and other earthworks such as roads and railways. Rockfill embankments are usually subjected to high pressure and repeated loading from vehicles and earthquake. To study the behaviour of rockfills, large-scale testing equipments were developed in some research centers (e.g. Sowers *et al.*, 1965; Fumagalli, 1969; Marachi *et al.*, 1969; Marsal, 1973), capable of performing most of the classical soil mechanics tests on rockfill specimens. The main conclusion drawn from all these experiments is that the mechanical properties of rockfills are closely related to breakage properties of rock particles (e.g. Oldecop and Alonso, 2001; Salim and Indraratna, 2004). In other words particle breakage has been identified to be the main reason for the differences observed between the behaviour of sand (at low and moderate stress levels) and rockfill material. Particle breakage in rockfill depends on the strength of individual particles, grain size distribution, stress level and the relative humidity prevailing in the rockfill voids (Chávez and Alonso, 2003).

The hyperbolic elastic model of Duncan and Chang (1970) has been the main tool for modelling different types of rockfill materials for about three decades. This model is based on the generalized Hooke's law and was proposed to simulate the nonlinear stress–strain behaviour of soils. Although it has been widely used mainly due to its simplicity and convenience, it can neither simulate the volumetric dilatancy of rockfills nor can it represent the particle breakage phenomenon which plays a distinct role in the behaviour of rockfills.

To model the cyclic and dynamic behavior of rockfills, viscoelastic models are traditionally used; these are typically equivalent linear models of Masing nonlinear models. Although these models are simple and can capture some features of dynamic response of rockfills, they cannot represent many aspects of nonlinear behaviour of rockfills such as strain softening, stress history and anisotropy. Generally, empirical relations need to be included in these models to

take into account the accumulation of permanent strains and generation of pore pressure (e.g. Martin *et al.* 1975).

Since 1970's, there has been extensive studies on development of elastoplastic models for monotonic and cyclic behaviour of soils. Great efforts have been devoted in modelling the cyclic behaviour of granular materials using advanced constitutive frameworks, such as bounding surface plasticity (e.g. Dafalias, 1986; Bardet, 1986; Khalili *et al.,* 2005) hypoplasticity (e.g. Gudehus, 1996; Bauer, 1996; Fu *et al.*, 2011), generalized plasticity (e.g. Pastor *et al.*, 1990; Ling and Yang, 2006), subloading surface plasticity (e.g. Hashiguchi, 1989; Kohgo *et al.*, 2007) and the disturbed state concept (e.g. Deasi, 1994; Varadarajan *et al.*, 2003).

Recently, a rigorous bounding surface model based on the concept of the critical state soil mechanics was developed at the University of New South Wales (UNSW) by Russell and Khalili (2004) to model the stress-strain behaviour of sands. Later Khalili *et al.* (2005 & 2008) extended the UNSW model to simulate the behaviour of sands subjected to cyclic loading under saturated and unsaturated states including hydraulic hysteresis effects. Kan *et al.* (2014) introduced a single stress point mapping rule for this model which has a simpler procedure and is more compliant to application to complex loading paths.

In the UNSW model, the position and evolution of the bounding surface is linked to the Limiting Isotropic Compression Line (LICL). To take into account the effect of the particle breakage on the mechanical behaviour of geomaterials, both LICL and the Critical State Line (CSL) are taken as two (Kan *et al.*, 2014) or three (Russell and Khalili, 2004) segmented lines. Both CSL and LICL are assumed to be fixed in a semi logarithmic compression plane. This assumption, which has been made based on the results of laboratory tests on sands, is revisited in this paper to be able to simulate the crushing phenomenon in rockfill materials. A novel approach in which the CSL and LICL are considered as translating curves is incorporated in the UNSW model. This approach significantly improves the capability of the model in simulating

the irrecoverable permanent strains due to particle breakage which occurs in cyclic loading of crushable materials. This is an important characteristic of crushable materials which could not be simulated easily in constitutive models with a fixed critical state line.

In this paper the governing equations for the proposed model are described and the method by which the translation of the CSL and LICL is related to particle crushing is introduced. A procedure is introduced to obtain the material parameters required for the proposed model. The proposed model is then used to simulate the behavior of rockfills with rounded and angular particles as well as ballast and coarse gravel to highlight the capabilities of the model. In addition to the conventional triaxial tests under monotonic loading, simulations are also performed under more complex stress paths as well as under cyclic loading to demonstrate the robustness of the model in simulating actual stress paths that may occur in real boundary value problems.

2. PRELIMINARIES

In the model presented here, the material behaviour is assumed isotropic and rate independent. Compression is considered positive. For the sake of simplicity, all derivations are presented in the $p'-q$ plane where p' and q are the mean effective stress and the deviatoric stress, respectively.

2.1. Critical state

The critical state (CS) is an ultimate condition towards which all states approach with increasing deviatoric shear strain. Traditionally, the critical state line has been chosen as linear in a semi logarithmic compression plane, that is, the specific volume, $\upsilon = 1+e$, versus the logarithm of the mean effective stress, $\ln p'$. Here a modified form of the critical state line is

introduced which has two curvatures and limits the minimum and maximum specific volumes corresponding to very large and very low stresses. The critical state is defined as:

$$\upsilon = \upsilon_{\min} + \left(\upsilon_{\max} - \upsilon_{\min}\right)\exp\left[-\left(p'/p_{cs}\right)^{\alpha_1}\right] \quad (1)$$

where $\upsilon_{\max}$ and $\upsilon_{\min}$ are the maximum and minimum specific volumes for a given particle grading and p_{cs} and α_1 are parameters which control the shape of the CSL.

To take into account the effects of crushing of soil particles at high stresses in the model, some investigators have assumed the CSL in the $\upsilon \sim \ln p'$ plane to take the form of two or three linear segments (e.g. Been *et al.*, 1991, Khalili *et al.*, 2005, Vilhar *et al.*, 2013). For highly crushable materials however, as the soil particles crush and efficiently fill the voids, the reference packing of the soil becomes denser. As a result, the maximum and minimum specific volumes fall correspondingly, and any soil properties linked with the reference packing, including the specific volume at critical state or isotropic compression state, will be affected. Therefore the critical state line will not retain its original position while crushing takes place (e.g. in Ghafghazi *et al*., 2014).

Muir Wood (2007) proposed a grading index (I_G) which represents the changes in particle grading and is defined as the ratio of the area under the current grain size distribution to the area under the fractal grading curve, where fractal is defined as the arrangement at which all particles look the same at all scales (McDowell *et al.*, 1996). This index is included into the proposed model to take into account the mechanical effects of the change in particle grading on specific volume. Compared to other indices proposed for particle breakage (e.g. breakage index as proposed by Hardin, 1985), I_G represents better the physical differences made due to the changes in grading since it incorporates the concept of fractal grading. Figure 1(a) shows the schematic diagram of an evolving grading and the definition of grading index. In Figure 1(b),

degradation in particle grading with increasing confining pressure and the evolution of fractal grading in a crushable material (crushed Cambric slate) are shown. In this study, the fractal grading curve, which represents the ultimate achievable grading is extracted according to the procedure outlined in McDowell *et al.* (1996) based on the theory of split probability.

Following Kikumoto *et al.* (2010), it is assumed that the values of $\upsilon_{\max}$ and $\upsilon_{\min}$ in equation (1) are dependent on the grading index I_G. As the grading index changes from that corresponding to single size particles $(I_G = 0)$ to that of the fractal grading $(I_G = 1)$, the minimum specific volume decreases from υ_l to 1 and the maximum specific volume decreases from υ_h to $\upsilon_{\max}$ by the same amount of $\upsilon_c (= \upsilon_l - 1)$ as:

$$\upsilon_{min} = \upsilon_l - \upsilon_c I_G \tag{2}$$

$$\upsilon_{\max} = \upsilon_h - \upsilon_c I_G \tag{3}$$

where υ_h and υ_l are the maximum and minimum specific volumes for the single sized particle grading $(I_G = 0)$. By substituting equations (2) and (3) into equation (1), the general form of the critical state can be obtained which includes the effects of the grading index on the position of the CSL as shown in Figure 2:

$$\upsilon = \upsilon_l - \upsilon_c I_G + (\upsilon_h - \upsilon_l) \exp\left[-\left(p'/p_{cs} \right)^{\alpha_1} \right] \tag{4}$$

Theoretically, when grading of a material approaches fractal grading $(I_G = 1)$ the void ratio approaches zero at very high stress level. In an idealized case, a packing of limiting grading is as efficient as the Apollonian fractal packing for which the specific volume is equal to unity because successively finer particles occupy the void spaces between coarser particles (Kasner and Supnick, 1943). However, this condition may never be reached in rockfill materials under practical stress ranges.

The CSL is defined in the $q \sim p'$ plane as a straight line with the slope of M_{cs}, which is related to the critical state friction angle, as

$$M_{cs} = \frac{6\sin\phi'_{cs}}{3\tilde{t} - \sin\phi'_{cs}} \tag{5}$$

where $\tilde{t} = +1$ represents compression and $\tilde{t} = -1$ extension. While a curved CSL in $q \sim p'$ plane as reported by Chávez and Alonso (2003) for a rockfill material is acknowledged, ϕ'_{cs} is considered independent of crushing of the particles, based on experimental observations made by many researchers (e.g. Coop, 1990; Been *et al.*,1991 and Russell and Khalili, 2004).

Some features of the model are linked to a dimensionless state parameter (ξ), defined as the vertical distance between the current state and the CSL in the $\upsilon \sim \ln p'$ plane (Figure 2). It is positive on the loose side of the critical state and expressed as

$$\xi = \upsilon - \upsilon_{cs} \tag{6}$$

where υ_{cs} is the specific volume at the critical state corresponding to the current p'.

2.2. Isotropic compression line

In the conventional soil mechanics, isotropic compression line (ICL) for critical state models is defined as a line in $\upsilon \sim \ln p'$ plane. In the proposed model, similar to the critical state line, a curved isotropic compression line is defined. For a constant grading and without considering the effects of particle crushing, this curve takes the form of

$$\upsilon = \upsilon_{\min} + \left(\upsilon^*_{\max} - \upsilon_{\min}\right)\exp\left[-\left(p'/p_{ic}\right)^{\alpha_1}\right] \tag{7}$$

where p_{ic} is a reference stress controlling the shape of the isotropic compression line and $\upsilon^{*}_{\max}$ is an adjustable parameter, introduced to ensure that the current state is always located on an ICL.

Figure 2 shows the shape of the ICL for a given stress state in $\upsilon \sim \ln p'$ plane. Incorporating equations (2) and (3) into equation (7), the general form of the ICL is obtained which includes the effect of particle crushing on the maximum and minimum specific volumes:

$$\upsilon = \upsilon_l - \upsilon_c I_G + \left(\upsilon^{*}_{\max} - \upsilon_l + \upsilon_c I_G\right)\exp\left[-\left(p'/p_{ic}\right)^{\alpha_1}\right] \qquad (8)$$

This relationship implies that as the reference specific volumes decrease and grading index increases due to the particle crushing, the isotropic compression line also moves downward in $\upsilon \sim \ln p'$ plane.

2.3. Limiting isotropic compression line

In addition to the critical state line, the constitutive model requires definition of a limiting isotropic compression line (LICL), in order to formulate hardening rule for the evolution of the yield/bounding surface. Similar to the critical state, LICL is a reference line in the $\upsilon \sim \ln p'$ plane where any stress state approaches under increasing isotropic compression. The isotropic compression line can also be regarded as the locus of the loosest possible state that a soil can achieve for a given mean effective stress.

In the model presented here, the limiting isotropic compression line is taken as a curve at a constant shift from CSL along the isotropic compression line in $\upsilon - \ln p'$ plane. A graphical depiction of LICL is shown in Figure 3a. Considering that point 1 is located on both CSL and the given ICL and point 2 is located on LICL and the same ICL, the following equation can be obtained for LICL:

$$\upsilon = \upsilon_l - \upsilon_c I_G + \left(\upsilon_h - \upsilon_l\right)\exp\left[-\left(\bar{p}'/Rp_{cs}\right)^{\alpha_1} + \left(\bar{p}'/Rp_{ic}\right)^{\alpha_1} - \left(\bar{p}'/p_{ic}\right)^{\alpha_1}\right] \qquad (9)$$

where R denotes the shift ratio in the $\upsilon \sim \ln p'$ plane and is a model parameter. Figure 3b shows a three dimensional presentation of the limiting isotropic compression surface where grading index is considered as an extra dimension along with the specific volume and the mean effective stress. This implies that any translation of the LICL is a function of particle crushing, i.e. LICL is not fixed in the $\upsilon - \ln p'$ plane as was originally proposed by Pestana and Whittle (1995). The idea of relocating LICL was also presented in Taiebat and Dafalias (2008) model for anisotropic sand, though they assumed the translation rule is explicitly a function of stress ratio (q / p').

2.4. Evolution of the grading index due to particle crushing

The grading index I_G, which varies from 0 for a single-sized grading to 1 for a limiting fractal grading, is a simple scalar representing the current grading. It increases as particle crushing occurs. The grading index describes the evolutions of mechanical properties due to particle crushing. An evolution law is necessary to be incorporated in the grading index in order to describe the effects of changes in grading in a soil model.

Hardin (1985) proposed a hyperbolic relationship between particle breakage and breakage stress based on experimental results, which can be written in terms of p' and q as:

$$\sigma'_b = p' \left[1 + \frac{2\sqrt{2}}{3} \left(\frac{q}{p'} \right)^3 \right] \tag{10}$$

Other researchers (e.g. Coop and Lee, 1993; Russell *et al.*, 2009) have also recognized the extent of particle crushing with stress level. Another approach is to relate the evolution of the grading index to total work or plastic work done on a volume of material (e.g. Miura and O-Hara, 1979; Lade *et al.*, 1996; Daouadji and Hicher, 2010). However, this approach shows

some deficiencies as it continuously changes the grading index to its fractal limit at the critical state regardless of the stress level.

In this research, the evolution of the grading index is assumed to be a function of the normalized stress. A function similar to the one proposed by Hardin (1985) is defined in the framework of the critical state used in the current work as:

$$p_{cr} = p'\left[1+\frac{1}{2}\left(\frac{q}{M_{cs}p'}\right)^3\right] \tag{11}$$

where p_{cr} describes the crushing stress at the current stress state and can be related to the grading index in the form of:

$$I_G = 1-\exp\left[-\left\langle\left(p_{cr}-p_{cr0}\right)/p_r\right\rangle^{\alpha_2}\right] \tag{12}$$

where p_{cr0} is the crushing stress for $I_G = 0$ and introduces the initiation of particle crushing, p_r is a reference stress and α_2 is a model parameter. Kikumoto *et al.* (2010) have used a similar form of the evolution of the grading index to define a second mechanism for yield due to crushing in their model. The crushing stress and the grading index increase as the material is loaded. Upon unloading and reloading, the crushing stress is kept unchanged as long as the maximum historic crushing stress is not attained. This feature ensures the capability of the model to capture the irrecoverable particle crushing in cyclic loading. Note that in the proposed model particle breakage is assumed to be independent of the shearing strain that may occur at constant stress state. This assumption is considered to be reasonable and valid for most of applications. Although some research, such as those of ring shear tests performed by Coop et al. (2004) on highly crushable carbonate sands, show that crushing also occurs at constant stress, it mainly occurs at shear strains larger than 200%. This range of strain is far beyond most of the practical range which is often less than 20%.

2.5. Elastic modulus

The elastic bulk modulus can be calculated from (8), assuming that unloading/reloading occurs along an isotropic compression line in the $\upsilon \sim \ln p'$ plane:

$$K = \frac{\upsilon}{\upsilon - \upsilon_l + \upsilon_c I_G} \frac{p_{ic}^{\alpha_1}}{\alpha_1} p'^{1-\alpha_1} \tag{13}$$

This form of stress dependency of the elastic moduli is similar to those suggested by many researchers, e.g. Gajo and Muir Wood (1999) and Kikumoto et al. (2010).

3. BOUNDING AND LOADING SURFACES

Accurate descriptions of the bounding surface are required in order to avoid complications in the stress–strain simulations of rockfills. The undrained response of the material at its loosest state is used to determine the shape of the bounding surface. Similar to the original UNSW bounding surface model (after Russell and Khalili, 2004), the shape of the bounding surface is taken as a tear drop and defined as:

$$F\left(\bar{p}', \bar{q}, \bar{p}_c'\right) = \left(\frac{\bar{q}}{M_{cs}\bar{p}'}\right)^N - \frac{\ln\left(\bar{p}_c'/\bar{p}'\right)}{\ln R} = 0 \tag{14}$$

$\bar{p}_c'$ is a function of the plastic volumetric strain and controls the size of the bounding surface. The material constant R represents the ratio of $\bar{p}_c'$ and the mean effective stress at the intercept of the bounding surface with CSL in the $q \sim p'$ space. The constant N controls the curvature of the bounding surface.

The loading and bounding surfaces are assumed to be of the same shape, and are homologous about the origin in the $q \sim p'$ plane during first time loading.

For unloading and reloading, the centre of homology moves to the last point of stress reversal. To maintain similarity with the bounding surface, the loading surfaces undergo kinematic hardening during loading and unloading such that they remain homologues with the bounding surface at the centre of homology. The image point for cyclic loading is located by simple radial projection of the stress point on the bounding surfaces passing through each point of stress reversal (Kan *et al.*, 2014). Figure 4 shows the shape of the loading surfaces for first time loading as well as unloading/reloading case, along with the radial mapping rule used to find the image point on the bounding surface.

4. PLASTIC POTENTIAL

The plastic potential defines the direction of the incremental plastic strain vectors. Using a generalization of the original Cam-clay dilation rule (Roscoe, Schofield and Thurairajah, 1963) and taking into account the dependency of dilatancy on the state parameter, the plastic potential (g) is defined as

$$g\left(p', q, p_o\right) = \tilde{t}q + \frac{AM_{cs}p'}{A-1}\left(\left(\frac{p'}{p_o}\right)^{A-1} - 1\right) \qquad A \neq 1 \qquad (15)$$

$$g\left(p', q, p_o\right) = \tilde{t}q + M_{cs}p'\ln\left(\frac{p'}{p_o}\right) \qquad A = 1 \qquad (16)$$

where p_0 controls the size of the plastic potential, though it is not required in the model calibration, since only derivatives of g are incorporated in formulations, and A is a material parameter. $\tilde{t}$ is a scalar, the sign of which controls the direction of plastic flow in the deviatoric plane.

It is assumed that the form of the plastic potential will be unaffected by the state of grading of crushable materials. Although it may be hard to imagine that a material with a uniform grading

has the same stress-dilatancy relationship as a material with a fractal grading, within the practical range of changes in grading the effect of grading on stress-dilatancy relationship is assumed to be very small and can be ignored in the formulation of plastic potential. This assumption is consistent with the results of investigation of Muir Wood and Maeda (2008) which shows that samples with the same density but different gradings have similar dilatancy. Kikumoto *et al.* (2010) also assumed that the effect of grading on plastic potential is negligible. On the contrary, Salim and Indraratna (2004) have included the effect of particle crushing on plastic potential of ballast material.

5. HARDENING MODULUS

As the usual approach in bounding surface, the hardening modulus h is divided into two components

$$h = h_b + h_f \tag{17}$$

where h_b is the plastic modulus at $\bar{\boldsymbol{\sigma}}'$ on the bounding surface, and h_f is plastic modulus at $\boldsymbol{\sigma}'$ and defined as a function of the distance between $\boldsymbol{\sigma}'$ and $\bar{\boldsymbol{\sigma}}'$. Applying the consistency condition at the bounding surface and assuming isotropic hardening of the bounding surface with plastic volumetric compression, h_b is calculated as

$$h_b = -\frac{\partial F}{\partial \bar{p}'_c}\frac{\partial \bar{p}'_c}{\partial \varepsilon_v^p}\frac{m_p}{\left\|\partial F/\partial \bar{\boldsymbol{\sigma}}'\right\|} \tag{18}$$

with $m_p = \dfrac{\partial g/\partial \bar{p}'}{\left\|\partial g/\partial \boldsymbol{\sigma}'\right\|}$.

In this way, any softening effect due to particle crushing is incorporated into plastic volumetric strain. Using the chain rule of differentiation, equation (18) can be rewritten as

$$h_b = \frac{\upsilon}{\left(\lambda^* - \kappa^* + \bar{p}_c' \upsilon_c \frac{\partial I_G}{\partial p_{cr}} \frac{\partial p_{cr}}{\partial \bar{p}_c'}\right) \ln R} \frac{m_p}{\left\| \partial F / \partial \bar{\boldsymbol{\sigma}}' \right\|} \tag{19}$$

where $\partial I_G / \partial p_{cr}$ can be calculated from equation (12), λ^* denotes the current slope of the LICL in the $\upsilon - \ln p'$ plane and κ^* is the current slope of the isotropic compression line. The following equation can be used to calculate the rate of $\partial p_{cr} / \partial \bar{p}_c'$:

$$\frac{\partial p_{cr}}{\partial \bar{p}_c'} = \frac{p_c'}{\bar{p}_c'} \left[1 - \left(\frac{\bar{q}}{M_{cs} \bar{p}'} \right)^3 \right] \left[\frac{\bar{p}'}{\bar{p}_c'} \frac{1}{1 + N \left(\frac{\bar{q}}{M_{cs} \bar{p}'} \right)^N \ln R} \right] + \frac{3}{2 M_{cs}} \frac{p_c'}{\bar{p}_c'} \left(\frac{\bar{q}}{M_{cs} \bar{p}'} \right)^{2-N} \frac{\bar{q}}{N \bar{p}_c'} \tag{20}$$

The modulus h_f is defined such that it is zero on the bounding surface and infinity at the point of stress reversal, and can take the form of:

$$h_f = \frac{\upsilon p'}{\lambda^* - \kappa^* + \bar{p}_c' \upsilon_c \frac{\partial I_G}{\partial p_{cr}} \frac{\partial p_{cr}}{\partial \bar{p}_c'}} \left(\frac{\bar{p}_c'}{p_c'} - 1 \right) k_m \left(\eta_p - \tilde{t} \eta \right) \tag{21}$$

where $\bar{p}_c'$ and p_c' define the sizes of the bounding and loading surfaces, respectively, η_p is the slope of the peak strength line in the $q \sim p'$ plane, and k_m is a scaling parameter controlling the steepness of the $q \sim \varepsilon_q$ curve. η_p is a function of the state parameter and the slope of the critical state line, which is given as

$$\eta_p = \tilde{t} \left(1 - k \xi \right) M_{cs} \tag{22}$$

where k is a material parameter. Following Kan *et al.* (2014), the scaling parameter k_m for granular materials is expressed as a function of the initial value of the dimensionless state parameter, ξ_0 and the initial confining pressure, p_0' :

$$k_m = k_{m0}\langle 1.0 - \beta_1 \exp(\xi_0)\rangle (p_0')^{\beta_2} \tag{23}$$

where k_{m0} , β_1 and β_2 are material parameters.

6. CALIBRATION OF MODEL PARAMETERS

The proposed bounding surface plasticity model, in its general form, requires: p_{ic} and ν to describe the elastic behaviour; M_{cs} (or ϕ_{cs}'), υ_l , υ_h , p_{cs} and α_1 to define the critical state line and its evolution with the particle crushing; N and R to define the shape of the bounding surface; α_2 , p_{cr0} and p_r to establish the evolution of the particle crushing and grading index with stress state; k to define the peak strength line; k_m to calibrate the hardening modulus; and A to define the stress-dilatancy relationship. The general form of the proposed model is applicable to any material which undergoes particle crushing and re-gradation during loading. However, a smaller number of parameters are required for crushable rocks, as some of the parameters were found to be constant.

The elastic parameters p_{ic} and ν with the critical state constants M_{cs} , υ_l , υ_h , p_{cs} and α_1 can be determined from triaxial tests using conventional procedures. p_{ic} is determined based on the shape of elastic unloading-reloading line on $\upsilon - \ln p'$ plane, and ν is the Poisson's ratio.

M_{cs} is the slope of the critical state line on the triaxial $q - p'$ plane. υ_l and υ_h , which are the minimum and maximum specific volumes for the single sized grading $(I_G = 0)$, p_{cs} and α_1 ,

by which the critical state lines in $\upsilon - \ln p'$ plane are described, can be also determined by the results of undrained triaxial compression tests.

The parameter N defines the shape of the bounding surface and can be determined by fitting the equation of the bounding surface to the effective stress path of undrained response of very loose samples. R is the distance between the CSL and LICL along the unloading/reloading line and can be determined from isotropic consolidation test data. Undrained tests on rockfill materials are not common in practice. Therefore, N and R were obtained based on simulation of a wide variety of different rockfill materials. It was found that constant values of 1.5 and 3.0 were sufficiently accurate for N and R, respectively.

The constitutive parameters α_2, p_{cr0} and p_r define the evolution of the grading index and can be determined by variation of the particle size distribution during isotropic or one-dimensional compression. Since granular materials exhibit particle crushing from very low stress levels, a constant value of $p_{cr0} = 1kPa$ is used throughout this research and results were found satisfactory.

Assuming that elastic strains are negligible in comparison to plastic strains, A is determined by plotting the stress ratio η against the measured total dilatancy in the standard drained triaxial compression tests. The value of k can be obtained from the slope of η_p / M_{cs} versus ξ. By examining test data for a range of soil samples, Gajo and Muir Wood (1999) suggested a constant value of $k = 2.0$ for all sandy soils. Examinations of test data in the current study showed that the same value can also be satisfactorily used for a wide range of rockfills with rounded to angular particles. k_m is strongly influenced by the initial state parameter ξ_0 and the loading direction (Khalili *et al.*, 2005). It is best obtained using the initial slope of drained loading/unloading responses in the $q - \varepsilon_q$ plane.

It can be seen that the required model parameters are reduced to 11 for crushable rockfill materials, all of which can be obtained by conventional experimental tests in the lab.

7. APPLICATION AND VERIFICATION

To demonstrate the performance of the model and the accuracy of its predictions, a series of simulations is performed using a host of triaxial tests conducted on a wide range of materials, including rockfills with round and angular particle shapes, crushed ballast and coarse gravel. Both conventional and non-conventional monotonic and complex cyclic loadings are simulated and the results are compared with experimental data. For monotonic tests, for each material at least four triaxial tests at different stress levels are used for simulations. Two of the tests, corresponding to the lowest and the highest initial mean stresses are used for calibration of the material parameters and then all tests are simulated using the same set of parameters. For Nuozadu rockfill, a total of eight tests with two different sets of stress paths are used in simulations. Set (1), stress paths #1 to #4 as shown in Figure 11, is used for both calibration and prediction and set (2), stress paths #5 to #8, is prediction only. For cyclic tests, calibration of the parameters is mainly based on the available monotonic test results, only k_m in unloading and reloading conditions is selected based on trial and error approach.

7.1. Performance under monotonic loading

7.1.1. Rockfills with round particles

- ***Ranjit Sagar alluvial rockfill***

Varadarajan *et al.* (2003) and Gupta (2009) have reported a series of drained triaxial tests on samples of Ranjit Sagar rockfill materials. This rockfill is alluvial consisting of rounded/subrounded particles up to 320 mm with sedimentary origin. Due to the size limits of

triaxial apparatus, particles with maximum grain size of 25, 50 and 80 mm were used in the experiments. In this study those tests performed on samples with maximum grain size of 80 mm are simulated to evaluate the performance of the model in reproducing the behaviour of highly coarse materials. Four conventional triaxial compression tests on samples with $\upsilon_0 = 1.16$ and $p_0' = 350, 700, 1100, 1400 kPa$ are simulated. The material parameters were all obtained using the procedures described before and are listed in Table 1 . The variation of the grading curves after the shearing phase, as reported by Abbas (2011), is used to obtain crushing parameters.

The results of the simulations are compared with the experimental data in Figure 5, in $q - \varepsilon_1$ and $\varepsilon_v - \varepsilon_1$ planes. The simulations result in smooth variations of deviatoric stress, q, and volumetric strain, ε_v, vs. axial strain, ε_1. In particular, the model captured well the higher volumetric contraction occurs under higher confining pressure, which is a specific feature of the behaviour of rockfill material. The predicted results for all four tests match the experimental data with an excellent accuracy.

- ***Shah Nehar riverbed rockfill***

Consolidated drained triaxial tests on Shah Nehar rockfill materials were conducted by Abbas (2003) and Varadarajan *et al.* (2006). This rockfill consists of micaceous sandstone and quartzite rocks with rounded particles, quarried from riverbed. Samples used in the experiments were obtained using parallel gradation technique where particles larger than 80 mm were sifted out. Four triaxial compression tests on samples with $\upsilon_0 = 1.27$ and $p_0' = 200, 400, 600, 800 kPa$ are simulated in this study. The material parameters used in the simulations are listed in Table 1.

Figure 6 shows the results of the simulations in $q-\varepsilon_1$ and $\varepsilon_v-\varepsilon_1$ planes, which shows an excellent agreement with the experimental data. The model predicts a reduction in the volume during shearing before exhibiting dilation for samples under lower confining pressures.

The excellent prediction of the model in simulations of Ranjit Sagar alluvial and Shah Nehar riverbed rockfills demonstrates its capability to depict the behaviour of rounded particle rockfills.

7.1.2. Rockfills with angular particles

- ***Purulia dam rockfill***

Varadarajan *et al.* (2003) and Gupta (2009) have reported the results of triaxial tests conducted on angular/subangular rockfill materials obtained from Purulia dam. This rockfill consists of metamorphic rock with minerals such as quartz, biotite and feldspar and has particle sizes as large as 1200 mm. However, the samples used in the experiment were produced from the same material with a maximum grain size of 80 mm and with a grading size distribution parallel to that of rockfill in the dam. The samples were prepared with an initial specific volume of $\upsilon_0 = 1.252$ and subjected to sharing with initial mean confining pressures of $p_0' = 300, 600, 900, 1200 kPa$. The material parameters used in the simulations are presented in Table 1.

The results of the simulations of these triaxial tests are compared with experimental data in Figure 7. In $q-\varepsilon_1$ plane, the general agreement between the simulated behaviour and experimental data is satisfactory. The model predicts higher deviatoric stresses in tests 3 and 4 which are under larger confining pressures. The predicted volumetric strains for all four tests are in good agreement with the experimental data. The tendency of the material for dilation after a peak contractive behaviour is captured throughout.

- ***Kol dam rockfill***

A series of consolidated drained triaxial tests on large size samples of quarried rockfill limestone used in construction of Kol dam in India has been reported in Abbas (2003) and Varadarajan et al. (2006). This material is of angular particles of up to 600 mm in size. Tests performed on samples with maximum grain size of 25 mm as reported in Varadarajan et al. (2006) are simulated in this study. Conventional triaxial compression tests were conducted on samples with relative density of 87% under initial mean effective pressures of $p_0' = 300$, 600, 900 and 1200 kPa. The material parameters obtained for this rockfill are listed in Table 1.

The results of the simulations are compared with those reported by Abbas (2003) in Figure 8 which shows an excellent agreement in both $q - \varepsilon_1$ and $\varepsilon_v - \varepsilon_1$ planes. Similar to Purulia rockfill, the Kol dam rockfill material tends to dilate after an initial contraction. Such a tendency is depicted in the form of increasing specific volume during shearing in $\upsilon - \ln p'$ plane, as shown in Figure 9 for test #4. Also shown in this figure are the shapes of the CSL and LICL and their translation with different values of grading index, I_G. This figure also shows that while softening occurs at the end of the shearing phase, the value of the grading index (I_G) remains unchanged and therefore in this phase CSL and LICL are both fixed in $\upsilon - \ln p'$ plane without any further translation.

- ***Crushed ballast***

Salim (2004) and Salim and Indraratna (2004) have reported a series of drained triaxial tests on samples of crushed latite ballast. The triaxial samples were 300 mm in diameter and 600 mm high. The latite basalt is a fine-grained, dense-looking black rock, mainly consisting of semi-angular crushed fragments of plagioclase and augite minerals. A maximum grain size of 53 mm was used in the experiments. Drained triaxial compression tests were performed on

samples with bulk unit weight of 15.4 to 15.6kN/m^3. The corresponding initial specific volume of the samples used in the simulations here were 1.707, 1.692, 1.658 and 1.645 for samples 1 to 4, with the initial mean effective pressure of 50, 100, 200 and $300kPa$, respectively. The material parameters used in the simulations are presented in Table 1.

The results of the simulations are compared with the experimental data in Figure 10. The behaviour of the crushed ballast in the triaxial experiments is very similar to rockfills with angular particles. However, the range of the stresses applied on the ballast is lower than the rockfills of Purulia and Kol dams. The performance of the model under lower range of stresses is as good as that under high stress range for rockfills, in both $q-\varepsilon_1$ and $\varepsilon_v-\varepsilon_1$ planes.

7.2. Complex stress paths

In this section the performance of the proposed model in simulating the behaviour of rockfill materials subjected to complex stress paths are investigated. Xiang *et al.* (2009) conducted a series of triaxial drained tests on rockfill materials, obtained from Nuozadu dam in China, under stress paths that could occur during construction, and during reservoir filling. This rockfill is of high quality with good durability and erosion resistance and with a maximum particle size of 800 mm. Samples used in the triaxial tests have particle sizes smaller than 60 mm and were prepared in a specimen of 655 mm high and 302 mm diameter. Xiang *et al.* assumed that the stress path during the construction of the dam can be approximated with a constant stress ratio (q/p'), while during the period of reservoir filling a transitional stress path with constant $\Delta q/\Delta p'$ is more appropriate. A total of 8 different tests are considered here for simulation purposes and their stress paths are shown in Figure 11. All samples are loaded with $\Delta q/\Delta p'=1.0$ to different mean effective stresses, p_1', in the first stage of loading. Then additional loading is applied on samples #1 to #4 with $\Delta q/\Delta p'=3.0$ (stress path 1), and on samples #5 to #8 with $\Delta q/\Delta p'=-1.5$ (stress path 2). All samples are reported to have the

same relative density with $\upsilon_0 = 1.32$. The material parameters used for the samples are presented in Table 2.

The results of the simulations of samples #1 to #4 under stress path (1) are shown in Figure 12. The agreement between the model predictions and the experimental data is very good, especially in tests #2 to #4. It should be noted that for test #1 the predicted results do not match with experimental data. However, using a hypoplastic constitutive model, Xiang *et al.* (2009) also could not obtain a good match even though they changed their model parameters with different ratios of stress increments.

Figure 13 shows the results of the simulations for stress path (2) applied on samples #5 to #8. These results demonstrate an excellent agreement with the experimental data. Apart from the peak deviatoric stress in test #5 which is predicted slightly less than that observed in the experiment, the general agreement seems satisfactory in $q - \varepsilon_1$ plane. In the volumetric strain plot, the dilative behaviour under smaller p_1' in tests #5 and #6 is captured well, as well as the contractive response of samples under larger p_1'.

In general, the results of the simulations for both stress paths show the excellent capability of the model in simulating the behaviour of the rockfill materials subjected to complex stress paths that expected to occur in rockfill dams.

7.3. Performance under cyclic loading

- ***Crushed Cambric slate***

Chávez and Alonso (2003) performed a series of triaxial drained tests on crushed Cambric slate, a rockfill material used in the construction of Jiloca dam in Spain. The material was obtained from a quarry and was further crushed and sieved so that the maximum particle size was 40 mm. These materials were subjected to triaxial drained tests conducted on samples with 250 mm

diameter and 500 mm height. Three of these tests are simulated here, with $\upsilon_0 = 1.60, 1.59, 1.55$ and initial mean effective stresses of $p_0' = 100, 300, 800 kPa$ respectively. Two of the tests are under monotonic loading while in the third test a cycle of unloading/reloading is also included in the stress path. The monotonic tests are used for calibration of the material parameters as the main focus here is on the cyclic test. The material parameters used in the simulations are listed in Table 2.

The predicted results of the simulations for monotonic and cyclic tests on Cambric slate are presented in Figure 14, together with the experimental data. Also shown in this figure are the results of simulations performed by Chávez and Alonso (2003) using a work hardening plasticity model. It can be seen that the predictions of the proposed model are very close to the experimental data, especially when they are compared to those predicted by Chávez and Alonso (2003). The advantage of the proposed model is more pronounced in predicting the volumetric strains. Chávez and Alonso (2003) found some difficulties in reproducing the volumetric response of the samples. Their model also underestimated dilation rates, especially for samples under low confining stresses. Chávez and Alonso (2003) referred this discrepancy to the viability of the critical state model for rockfill materials. However such a problem is completely resolved by the proposed model and the volumetric strains are predicted with an excellent accuracy in the current work (Figure 14). Apart from monotonic tests 1 and 2, the simulation of test with a single large cycle of unloading/reloading stress path also replicates the experimental data in both $q - \varepsilon_1$ and $\varepsilon_v - \varepsilon_1$ plots.

- ***Chiba gravel***

Maqbool and Koseki (2010) examined the effect of compaction on the behaviour of large samples of Chiba gravel by conducting a series of monotonic and cyclic triaxial compression tests. The gravel is hard and angular, consisting of crushed sandstones which can be categorized

as well-graded sandy gravel with maximum particle size of 38 mm. One of the cyclic tests conducted on this material is used here for simulation purposes. In this test, labeled as TC-5, a sample with an initial density of 1900 Kg/m^3 and $\upsilon_0 = 1.426$ was first subjected to isotropic compression to a mean effective stress of $p'_0 = 98kPa$, then sheared monotonically before cyclic loading. In the cyclic loading phase, 100 cycles of loading/unloading with a frequency of 0.001 Hz were applied by changing the deviatoric stress from 50kPa to 450kPa. After application of the cyclic loading the sample was sheared to failure under monotonic loading to study the post cyclic behavior of the gravel.

The loading history was simulated in this research using the material parameters listed in Table 2.The material parameters were calibrated using one of the monotonic tests conducted on this material. Note that the proposed model is rate independent and therefore the frequency of loading does not play any role in the simulations.

The results of the simulation for test TC-5 are compared with experimental data in Figure 15. An excellent agreement between the simulation results and the experimental data has been obtained. The deviatoric stress during monotonic loading and the post cyclic stage are both predicted with a very good accuracy. In the volumetric strain vs. axial strain plot, the dilative behaviour in pre and post cyclic stages and the contractive behaviour during cyclic loading are captured satisfactorily by the model.

8. CONCLUSION

A bounding surface plasticity model was introduced in this paper that can be used to simulate the behaviour of rockfill materials. A distinct feature of rockfill materials is believed to be particle crushing which governs some aspects of their response under monotonic and cyclic loading, such as the nonlinear dependency of strength and dilation on the confining pressure as

well as the accumulation of permanent strains during cyclic loading. In this study the particle breakage is treated using a translating critical state line, accompanied by a moving limiting isotropic compression line, both defined as functions of the particle breakage index, I_G. The framework of the UNSW bounding surface plasticity model was modified to incorporate these features and to take into account the effects of the particle breakage on the mechanical behaviour of rockfill materials. Although the model requires 15 model parameters, it was shown that 4 of the parameters (N, R, p_{cr0}, k) can be taken as constant and only 11 parameters need to be obtained from conventional triaxial tests. The accuracy and the robustness of the model were demonstrated through simulations of monotonic and cyclic loading on samples of different types of rockfills under drained and undrained conditions. Samples from both rounded and angular/subangular particles were considered in the simulations. Other types of highly crushable materials such as crushed ballast and crushed latite slate were also used in the simulations. The results of the simulations were invariably in excellent agreement with the experimental data. The model captures the characteristic features of the behaviour of different crushable granular materials for a wide range of densities and stresses. These features include stress softening and more pronounced dilatancy during drained loading under low confining pressures, stress hardening and contractive behaviour under higher confining pressures, as well as work hardening in stress-strain relationships and post cyclic strength. The versatility of the model in simulation of complex stress paths was demonstrated using two sets of unconventional stress paths which are expected to occur in rockfill shells of earth dams during construction and reservoir filling. All the predictions obtained by the model agree very well with the experimental data, which indicates the capability of the model in reproducing the fundamental strength and dilatancy behaviour of rockfill materials.

9. REFERENCES

Abbas, S. (2003). *Testing and modeling the behavior of riverbed and quarried rockfill materials.* Ph. D. thesis, IIT Delhi, New Delhi, India.

Abbas, S. M. (2011). *Constitutive Modeling of Rockfill Materials: Based on Index Properties*. Berlin, Germany: LAP LAMBERT Academic Publishing.

Bardet, J. (1986). Bounding surface plasticity model for sands. *Journal of Engineering Mechanics, 112*(11), 1198-1217.

Bauer, E. (1996). Calibration of a comprehensive hypoplastic model for granular materials. *Soils and Foundations, 36*(1), 13-26.

Been, K., Jefferies, M., & Hachey, J. (1991). The critical state of sands. *Geotechnique, 41*(3), 365-381.

Chávez, C., & Alonso, E. (2003). A constitutive model for crushed granular aggregates which includes suction effects. *Soils and Foundations, 43*(4), 215-227.

Coop, M. R. (1990). The mechanics of uncemented carbonate sands. *Geotechnique, 40*(4), 607-626.

Coop, M. R., & Lee, I. K. (1993). *The behaviour of granular soils at elevated stresses.* Predictive soil mechanics, Proc. C.P. Wroth Memorial Symposium, London.

Coop, M., Sorensen, K., Freitas, T. B., & Georgoutsos, G. (2004). Particle breakage during shearing of a carbonate sand. *Géotechnique, 54*(3), 157-163.

Dafalias, Y. F. (1986). Bounding surface plasticity: I: mathematical foundation and hypoplasticity. *Journal of Engineering Mechanics, ASCE, 112*(9), 966-987.

Daouadji, A., & Hicher, P. Y. (2010). An enhanced constitutive model for crushable granular materials. *International Journal for Numerical and Analytical Methods in Geomechanics, 34*(6), 555-580.

Desai, C. (1994). *Hierarchical single surface and the disturbed state constitutive models with emphasis on geotechnical applications.* Geoteehnical engineering: emerging trends in design and practice, ed. K.R. Saxena (Balkema).

Duncan, J. M., & Chang, C. Y. (1970). Nonlinear analysis of stress and strain in soils. *Journal of the Soil Mechanics and Foundations Division, 96*(5), 1629-1653.

Fu, Z. Z., Liu, S. H., & Gu, W. X. (2011). Evaluating the Wetting Induced Deformation of Rockfill Dams Using a Hypoplastic Constitutive Model. *Advanced Materials Research,* 243, 4564-4568.

Fumagalli, E. (1969). Tests on cohesionless materials for rockfill dams. *Journal of Soil Mechanics & Foundations Div., ASCE, 95*(No. SM1), 313-330.

Gajo, A., & Wood, D. M. (1999). Severn-Trent sand: a kinematic-hardening constitutive model: the qp formulation. *Geotechnique, 49*(5), 595-614.

Ghafghazi, M., Shuttle, D., & DeJong, J. (2014). Particle breakage and the critical state of sand. *Soils and Foundations, 54*(3), 451-461.

Gudehus, G. (1996). A comprehensive constitutive equation for granular materials. *Soils and Foundations, 36*(1), 1-12.

Gupta, A. K. (2009). Triaxial Behaviour of Rockfill Materials. *Electronic Journal of Geotechnical Engineering, 14*.

Hardin, B. O. (1985). Crushing of soil particles. *Journal of Geotechnical Engineering, 111*(10), 1177-1192.

Hashiguchi, K. (1989). Subloading surface model in unconventional plasticity. *International Journal of Solids and Structures, 25*(8), 917-945.

Kan, M. E., Taiebat, H. A., & Khalili, N. (2014). Simplified Mapping Rule for Bounding Surface Simulation of Complex Loading Paths in Granular Materials. *International Journal of Geomechanics, 14*(2), 239–253.

Kasner, E., & Supnick, F. (1943). The Apollonian packing of circles. *National Academy of Science, 29*(11), 378-384.

Khalili, N., Habte, M., & Valliappan, S. (2005). A bounding surface plasticity model for cyclic loading of granular soils. *International journal for numerical methods in engineering, 63*(14), 1939-1960.

Khalili, N., Habte, M., & Zargarbashi, S. (2008). A fully coupled flow deformation model for cyclic analysis of unsaturated soils including hydraulic and mechanical hystereses. *Computers and Geotechnics, 35*(6), 872-889.

Kikumoto, M., Muir Wood, D., & Russell, A. (2010). Particle crushing and deformation behaviour. *Soils and Foundations, 50*(4), 547-563.

Kohgo, Y., Asano, I., & Hayashida, Y. (2007). An elastoplastic model for unsaturated rockfills and its simulations of laboratory tests. *Soils and Foundations, 47*(5), 919-929.

Lade, P. V., Yamamuro, J. A., & Bopp, P. A. (1996). Significance of particle crushing in granular materials. *Journal of Geotechnical Engineering, 122*(4), 309-316.

Ling, H. I., & Yang, S. (2006). Unified sand model based on the critical state and generalized plasticity. *Journal of Engineering Mechanics, 132*(12), 1380-1391.

Maqbool, S., & Koseki, J. (2010). Large-scale triaxial tests to study effects of compaction energy and large cyclic loading history on shear behavior of gravel. *Soils and Foundations, 50*(5), 633-644.

Marachi, N. D., Chan, C. K., Seed, H. B., & Duncan, J. M. (1969). Strength and deformation characteristics of rockfill materials. Department of Civil Engineering: Report No. TE-69-5, University of California.

Marsal, R. J. (1973). Mechanical properties of rockfill. In R. C. H. S. J. Poulos (Ed.), *Embankment dam engineering, Casagrande volume* (pp. 109-200). New York: John Wiley & Sons.

Martin, G. R., Seed, H. B., & Finn, W. (1975). Fundamentals of liquefaction under cyclic loading. *Journal of the Geotechnical Engineering Division, 101*(5), 423-438.

McDowell, G. R., Bolton, M. D., & Robertson, D. (1996). The fractal crushing of granular materials. *Journal of the Mechanics and Physics of Solids, 44*(12), 2079-2101.

Miura, N., & O-Hara, S. (1979). Particle-crushing of a decomposed granite soil under shear stresses. *Soils and Foundations, 19*(3), 1-14.

Muir Wood, D. (2007). The magic of sands:The 20th Bjerrum Lecture presented in Oslo 25 November 2005. *Canadian Geotechnical Journal, 44*(11), 1329-1350.

Muir Wood, D., & Maeda, K. (2008). Changing grading of soil: effect on critical states. *Acta Geotechnica, 3*(1), 3-14.

Oldecop, L. A., & Alonso, E. E. (2001). A model for rockfill compressibility. *Geotechnique, 51*(2), 127-139.

Pastor, M., Zienkiewicz, O., & Chan, A. (1990). Generalized plasticity and the modelling of soil behaviour. *International Journal for Numerical and Analytical Methods in Geomechanics, 14*(3), 151-190.

Pestana, J. M., & Whittle, A. (1995). Compression model for cohesionless soils. *Geotechnique, 45*(4), 611-631.

Roscoe, K., Schofield, A., & Thurairajah, A. (1963). Yielding of clays in states wetter than critical. *Geotechnique, 13*(3), 211-240.

Russell, A. R., & Khalili, N. (2004). A bounding surface plasticity model for sands exhibiting particle crushing. *Canadian Geotechnical Journal, 41*(6), 1179-1192.

Russell, A. R., Muir Wood, D., & Kikumoto, M. (2009). Crushing of particles in idealised granular assemblies. *Journal of the Mechanics and Physics of Solids, 57*(8), 1293-1313.

Salim, M. W. (2004). *Deformation and degradation aspects of ballast and constitutive modelling under cyclic loading.* Ph. D. thesis, Faculty of Engineering, University of Wollongong.

Salim, W., & Indraratna, B. (2004). A new elastoplastic constitutive model for coarse granular aggregates incorporating particle breakage. *Canadian Geotechnical Journal, 41*(4), 657-671.

Sowers, G. F., Williams, R. C., & Wallace, T. S. (1965). Compressibility of broken rock and the settlement of rockfills. *6th ICSMFE, 2*.

Taiebat, M., & Dafalias, Y. F. (2008). SANISAND: Simple anisotropic sand plasticity model. *International Journal for Numerical and Analytical Methods in Geomechanics, 32*(8), 915-948.

Varadarajan, A., Sharma, K., Venkatachalam, K., & Gupta, A. (2003). Testing and modeling two rockfill materials. *Journal of Geotechnical and Geoenvironmental Engineering, ASCE, 129(3)*, 206-218.

Varadarajan, A., Sharma, K., Abbas, S., & Dhawan, A. (2006). Constitutive model for rockfill materials and determination of material constants. *International Journal of Geomechanics, ASCE, 6(4)*, 226-236.

Vilhar, G., Jovičić, V., & Coop, M. R. (2013). The role of particle breakage in the mechanics of a non-plastic silty sand. *Soils and Foundations, 53*(1), 91-104.

Xiang, B., Zhang, Z., & Chi, S. (2009). An improved hypoplastic constitutive model of rockfill considering effect of stress path. *Journal of Central South University of Technology, 16*(6), 1006-1013.

List of Figures

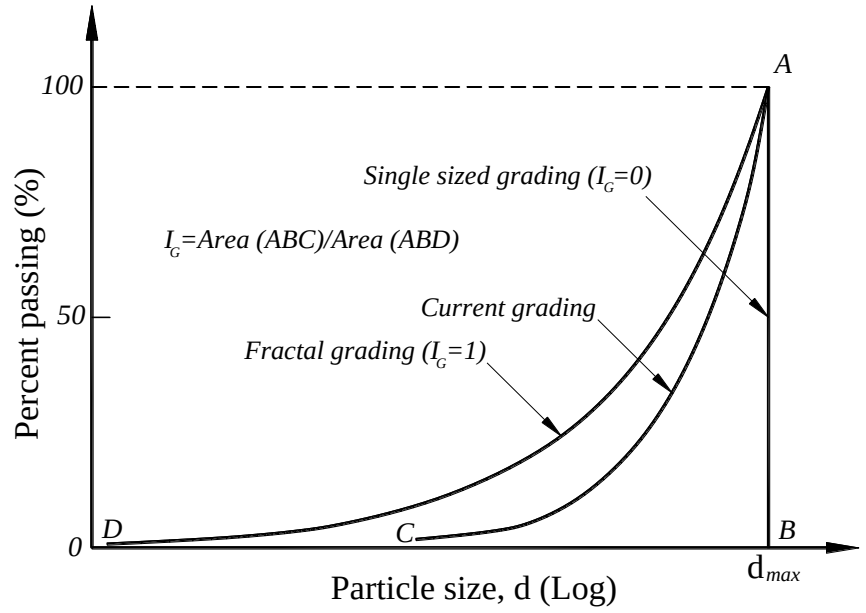

(a)

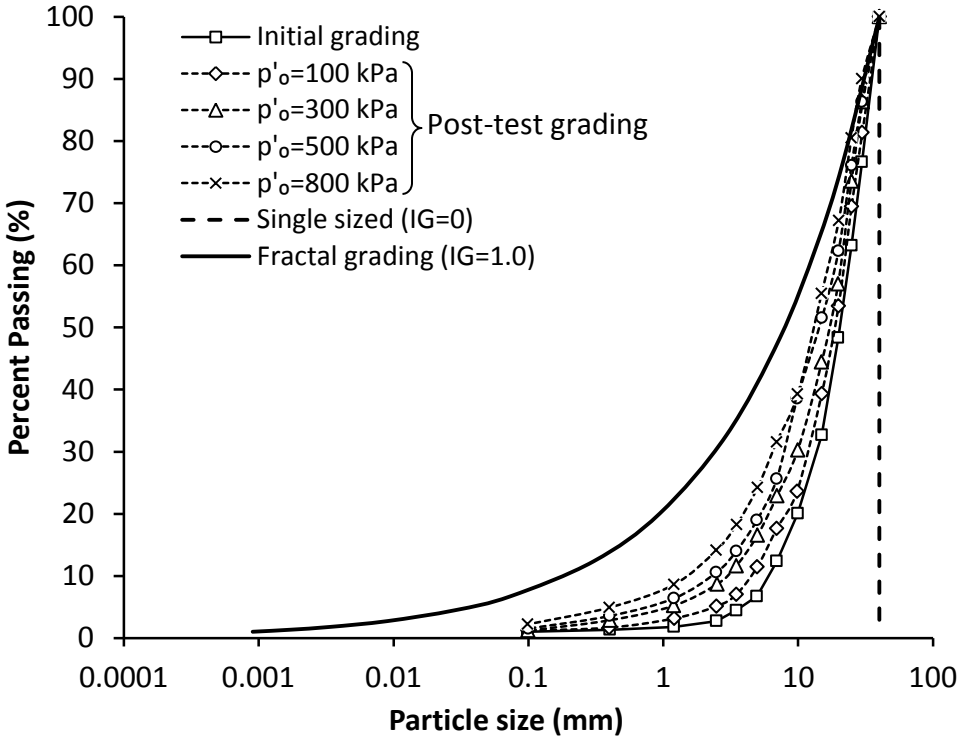

(b)

Figure 1: (a) Definition of grading index, I_G and evolution of grading and (b) an example of grading degradation and fractal grading for a rockfill (data after Chávez and Alonso, 2003)

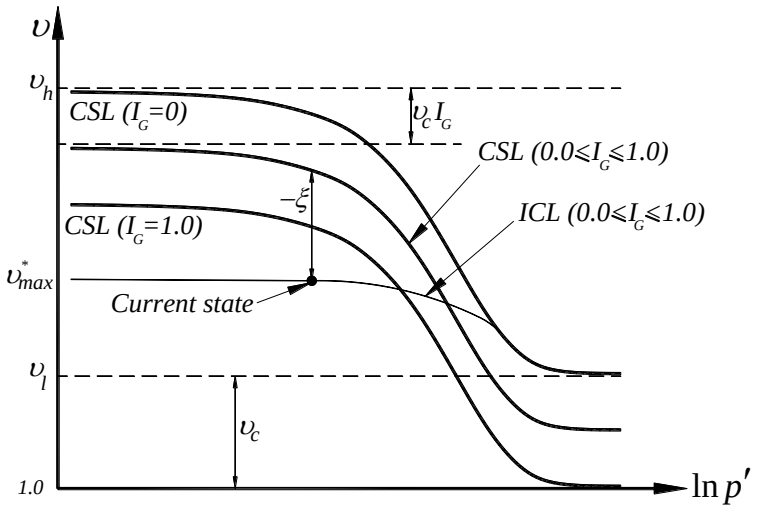

Figure 2: Critical State Line (CSL) and Isotropic Compression Lines (ICL) for different values of of I_G.

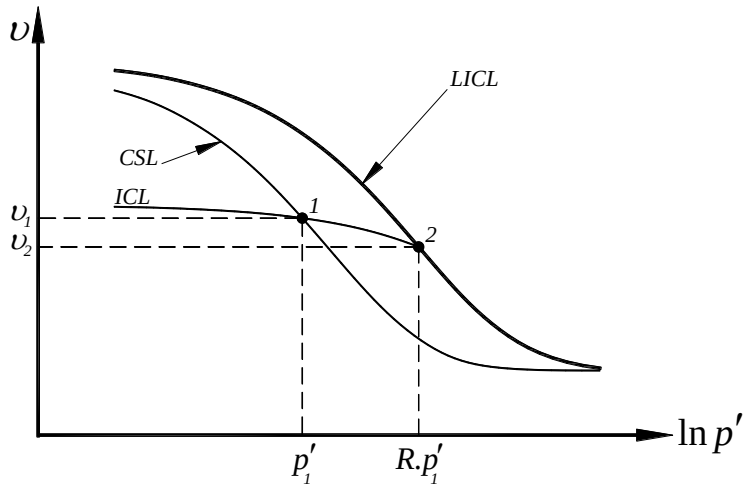

(a)

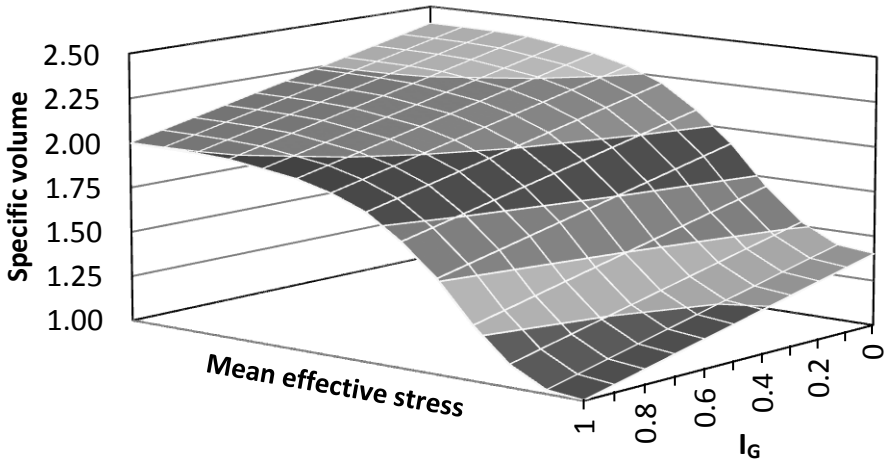

(b)

Figure 3: Location of Limiting Isotropic Compression Line (LICL) with constant I_G (a); presentation of LICL in 3D space (b)

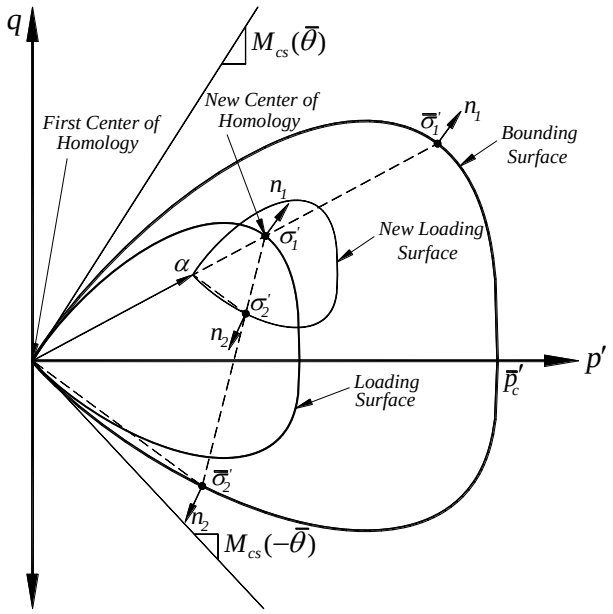

Figure 4: Loading surfaces and mapping rule for first time loading (path 0-1) and unloading (path 1-2)

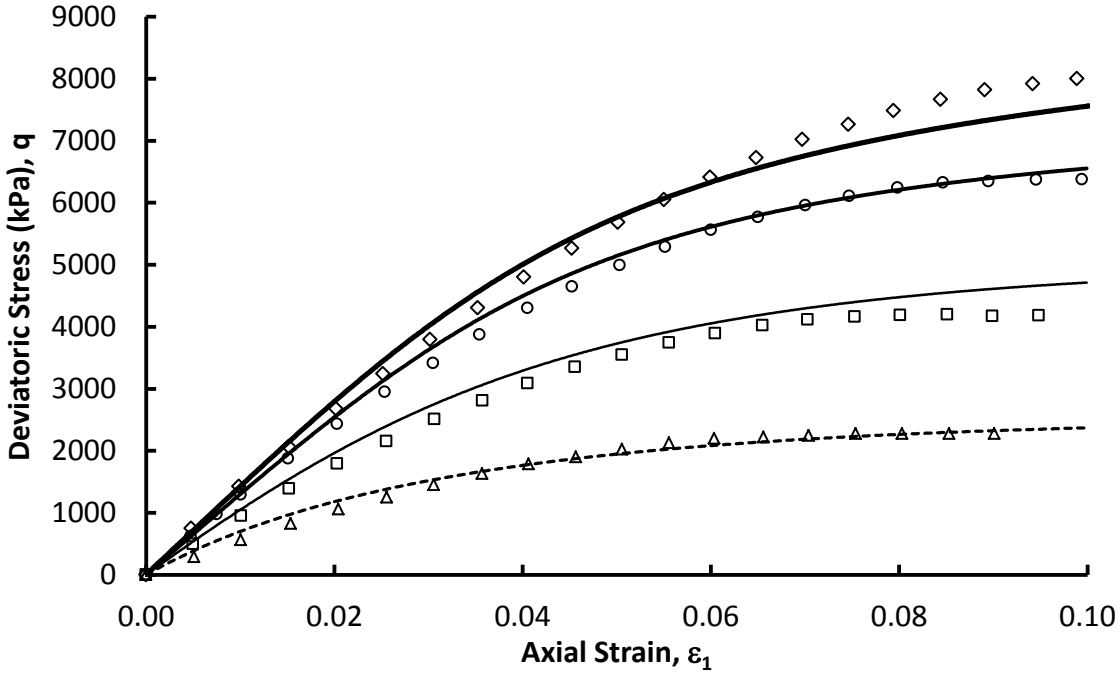

(a)

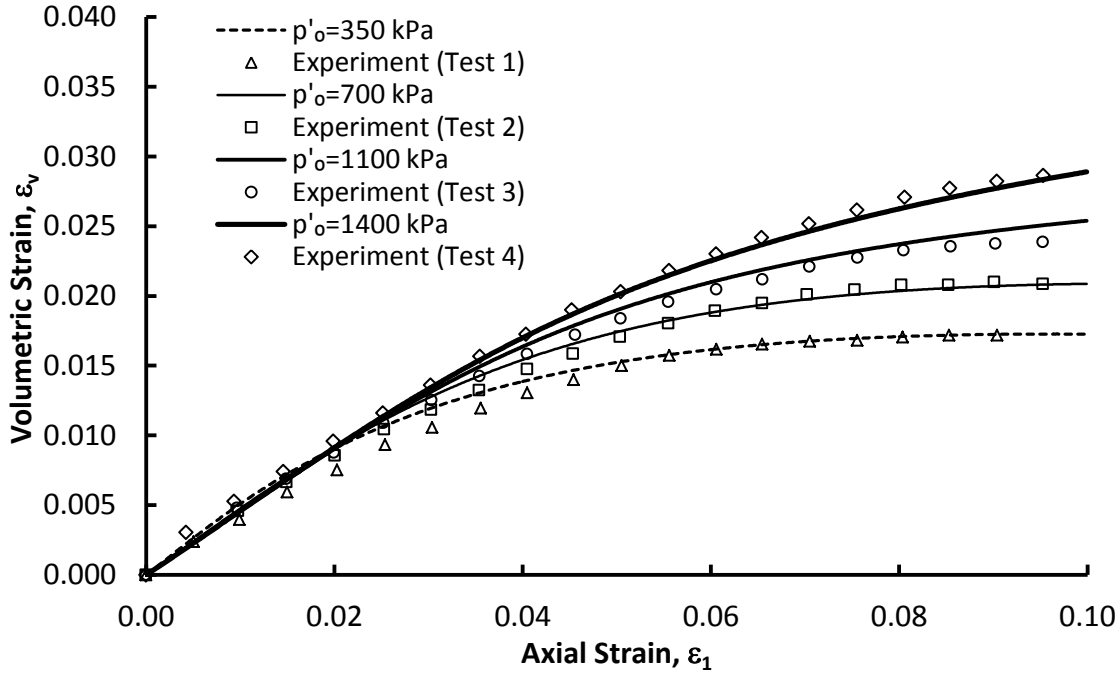

(b)

Figure 5: Triaxial compression tests on Ranjit Sagar rockfill (a) $q-\varepsilon_1$ plot and (b) $\varepsilon_v-\varepsilon_1$ plot

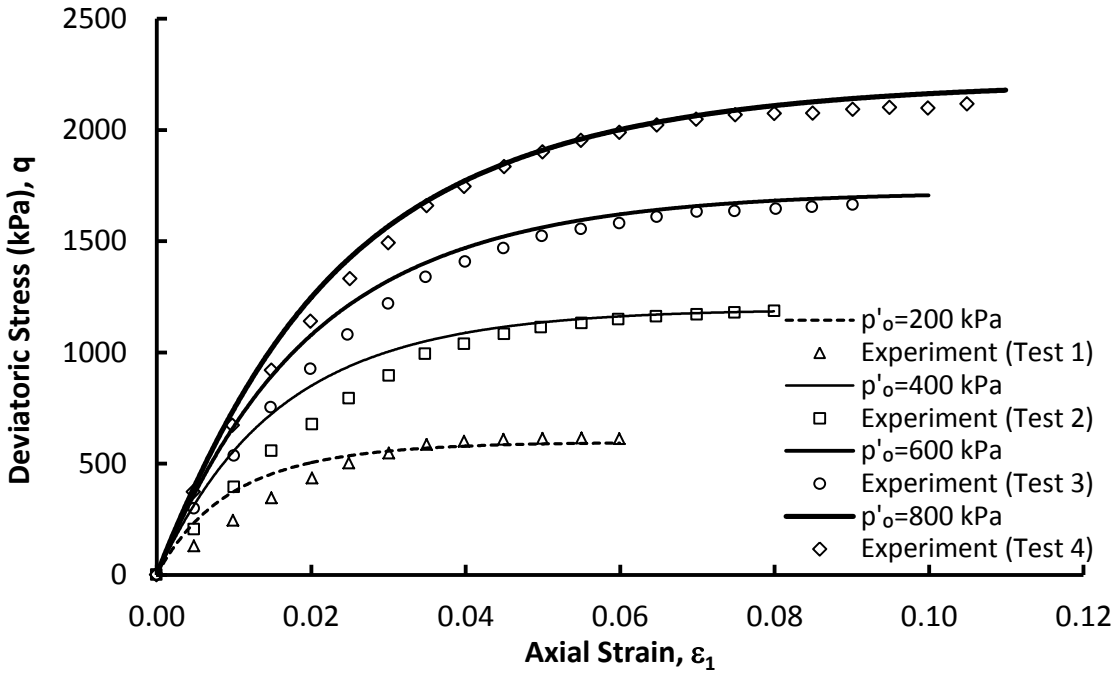

(a)

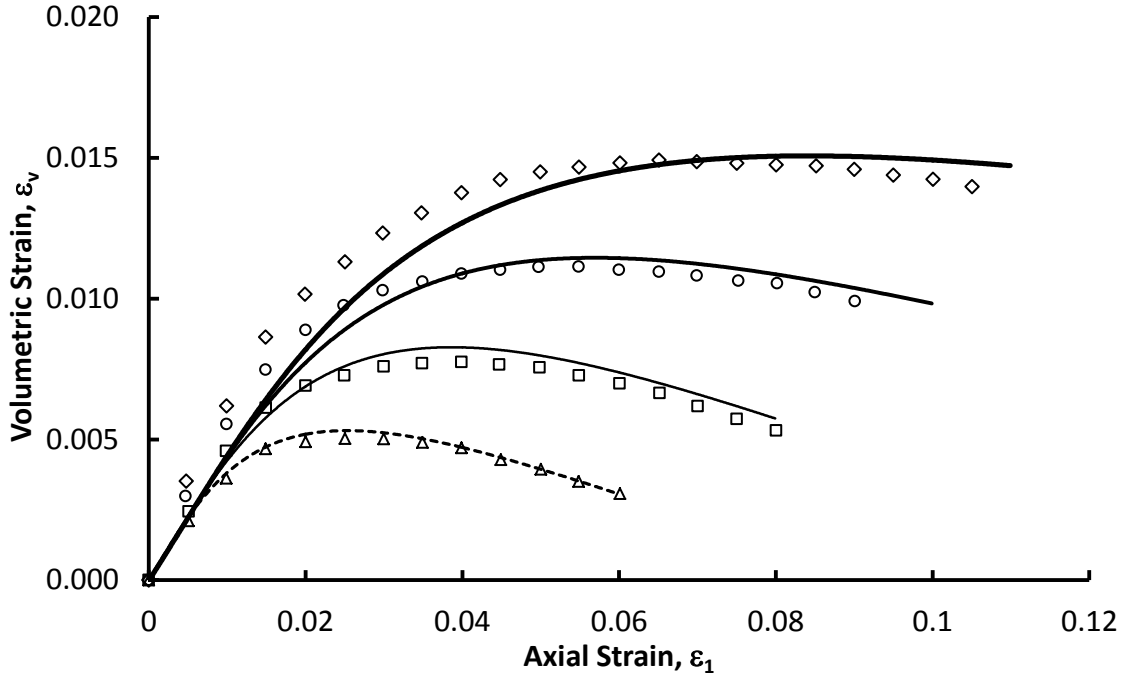

(b)

Figure 6: Triaxial compression tests on Shah Nehar rockfill (a) $q-\varepsilon_1$ plot and (b) $\varepsilon_v-\varepsilon_1$ plot

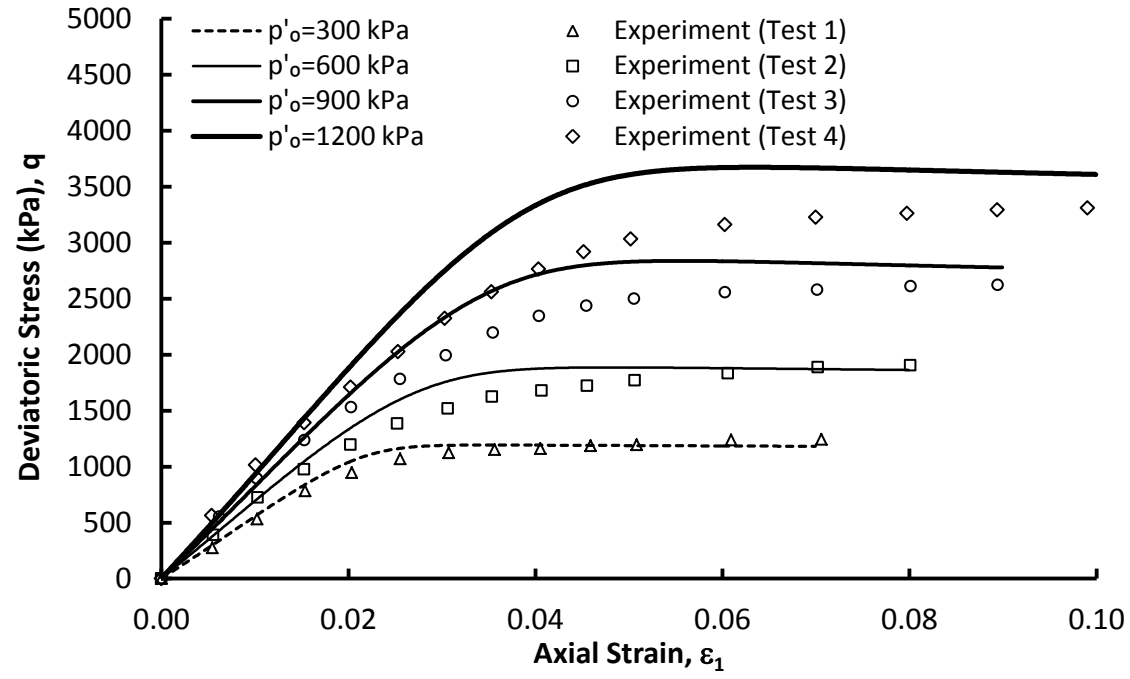

(a)

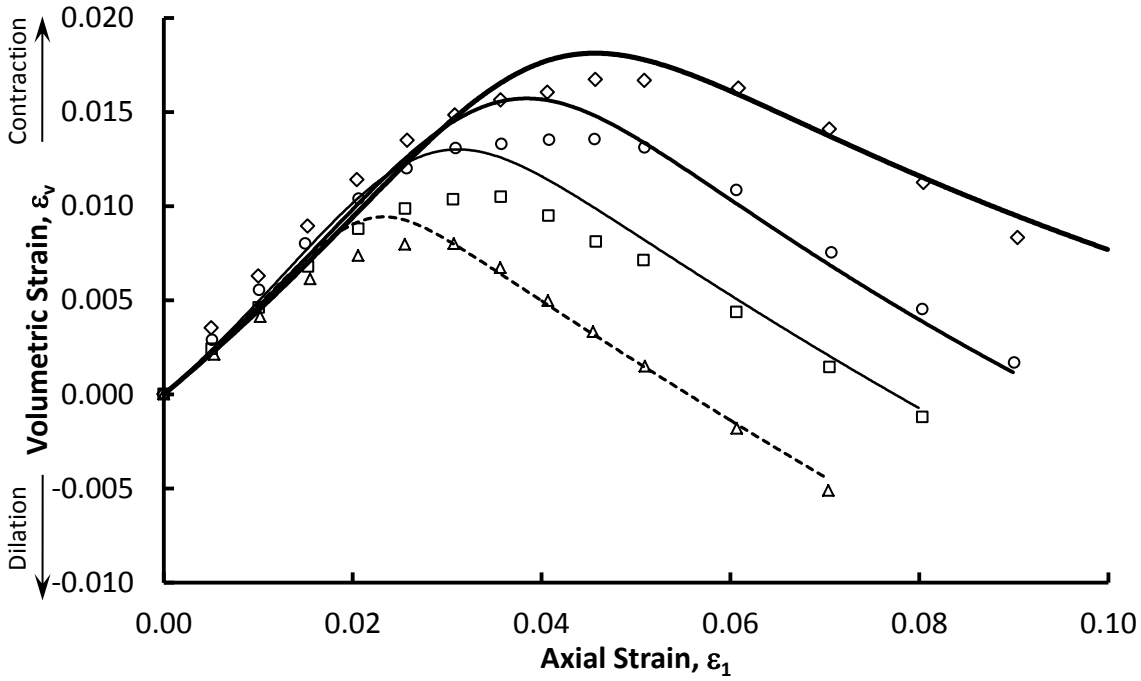

(b)

Figure 7: Triaxial compression tests on Purulia dam rockfill (a) $q-\varepsilon_1$ plot and (b) $\varepsilon_v-\varepsilon_1$ plot

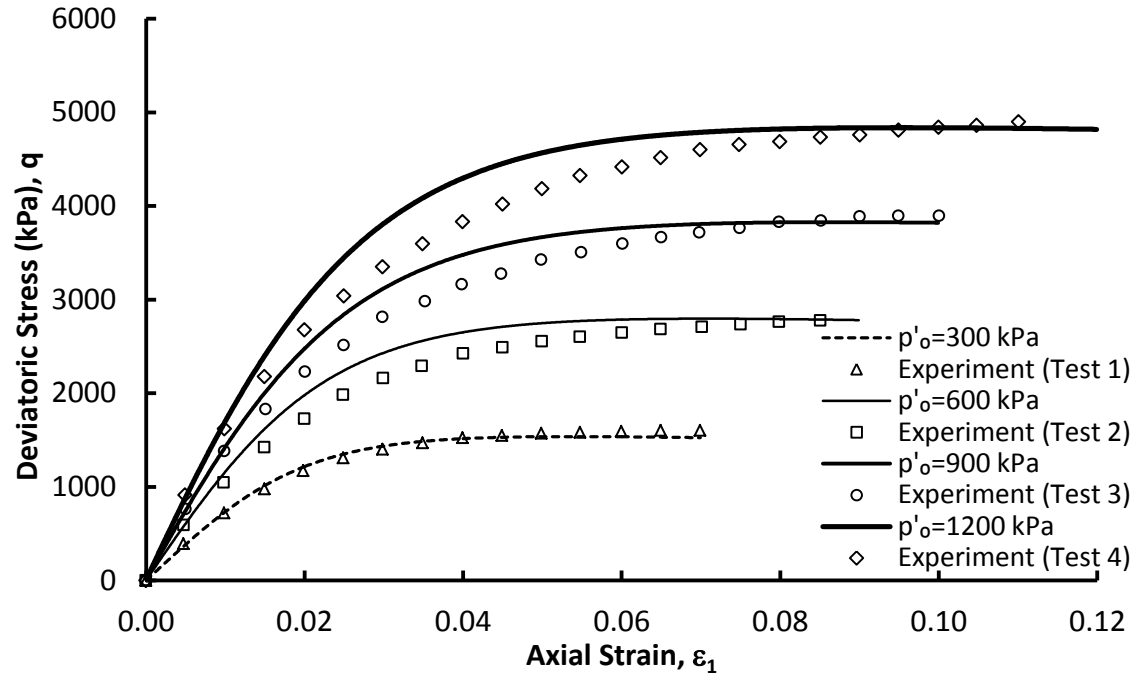

(a)

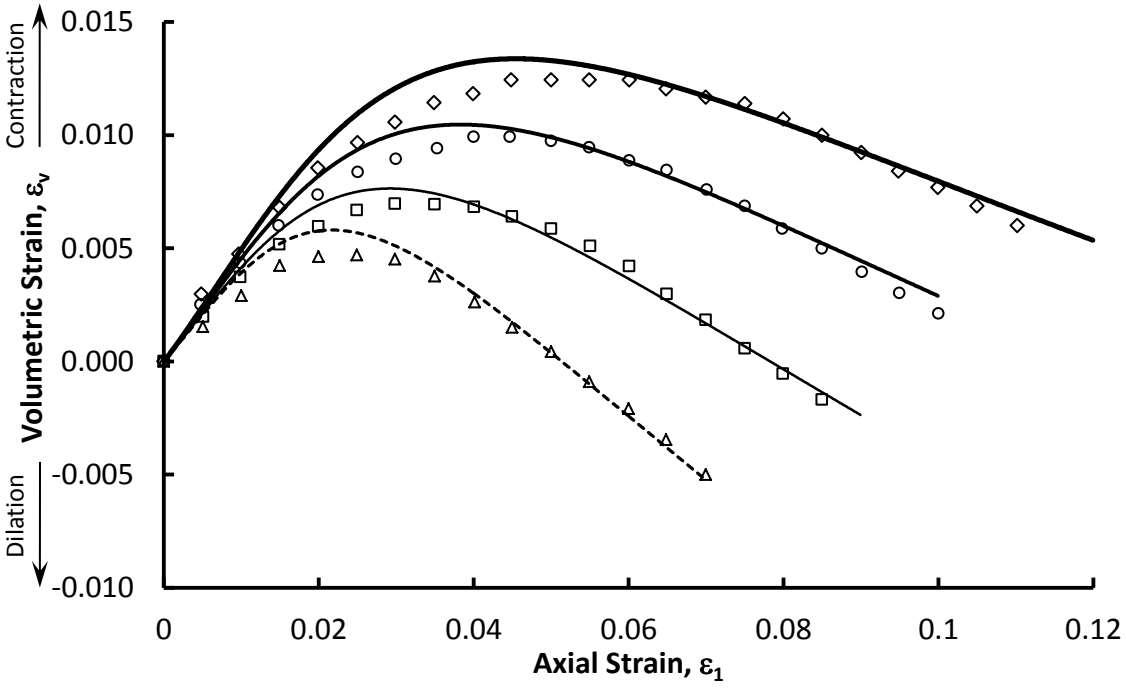

(b)

Figure 8: Triaxial compression tests on Kol dam rockfill (a) $q-\varepsilon_1$ plot and (b) $\varepsilon_v-\varepsilon_1$ plot

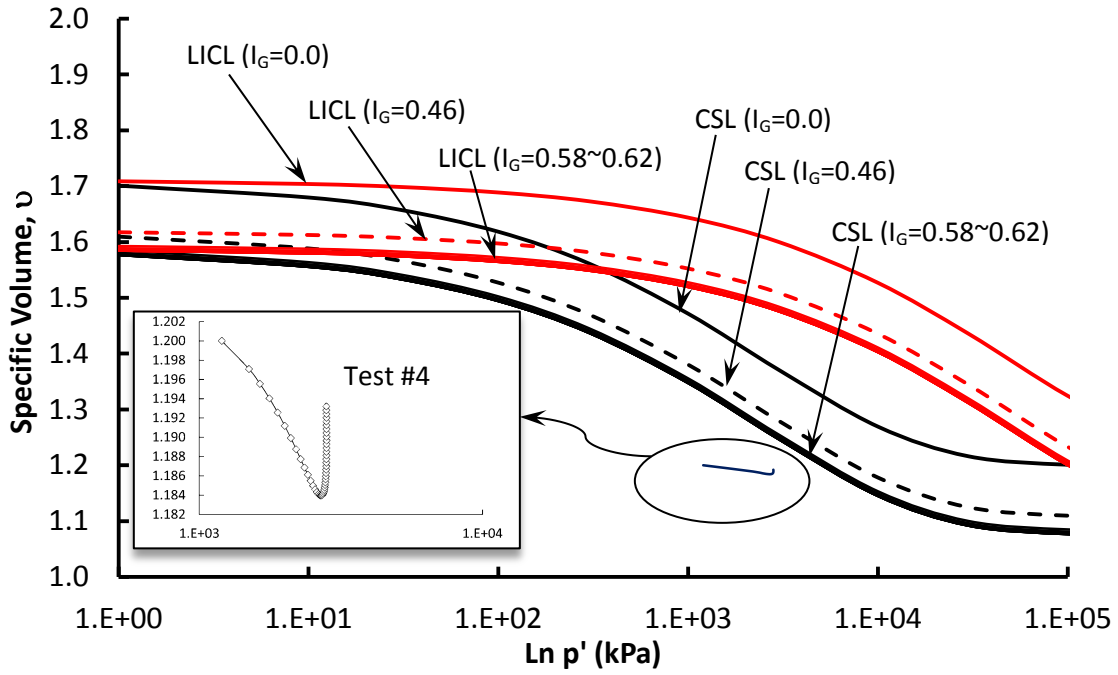

Figure 9: Variation of specific volume versus mean effective pressure and location of CSL and LICL in triaxial test #4 on Kol dam rockfill

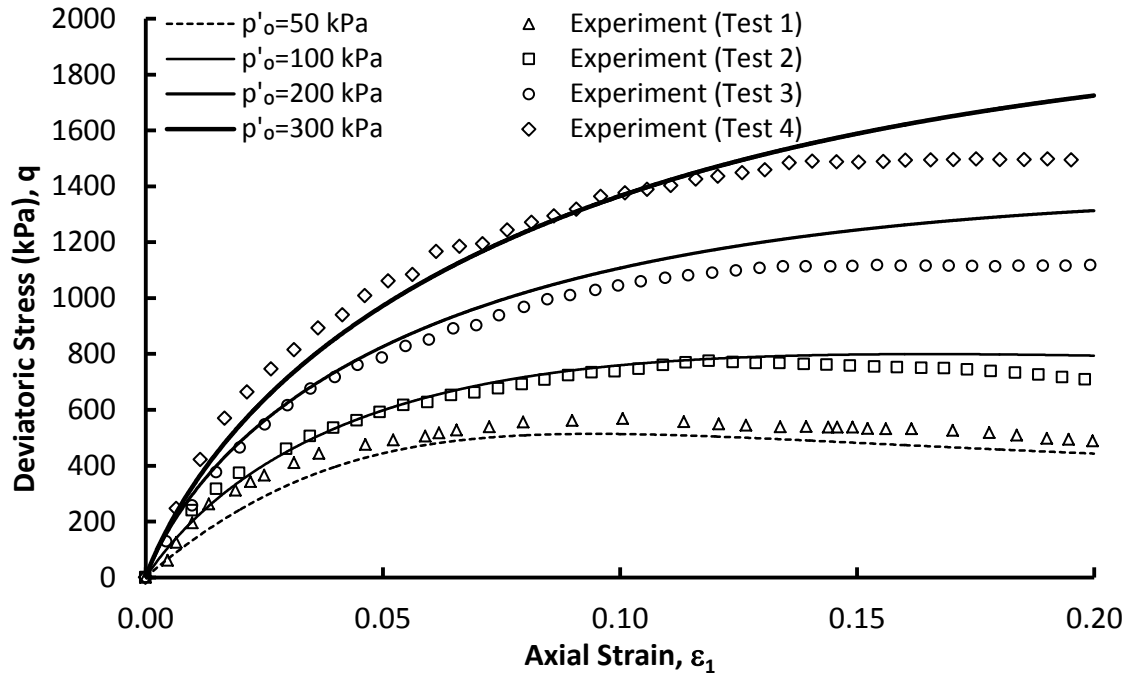

(a)

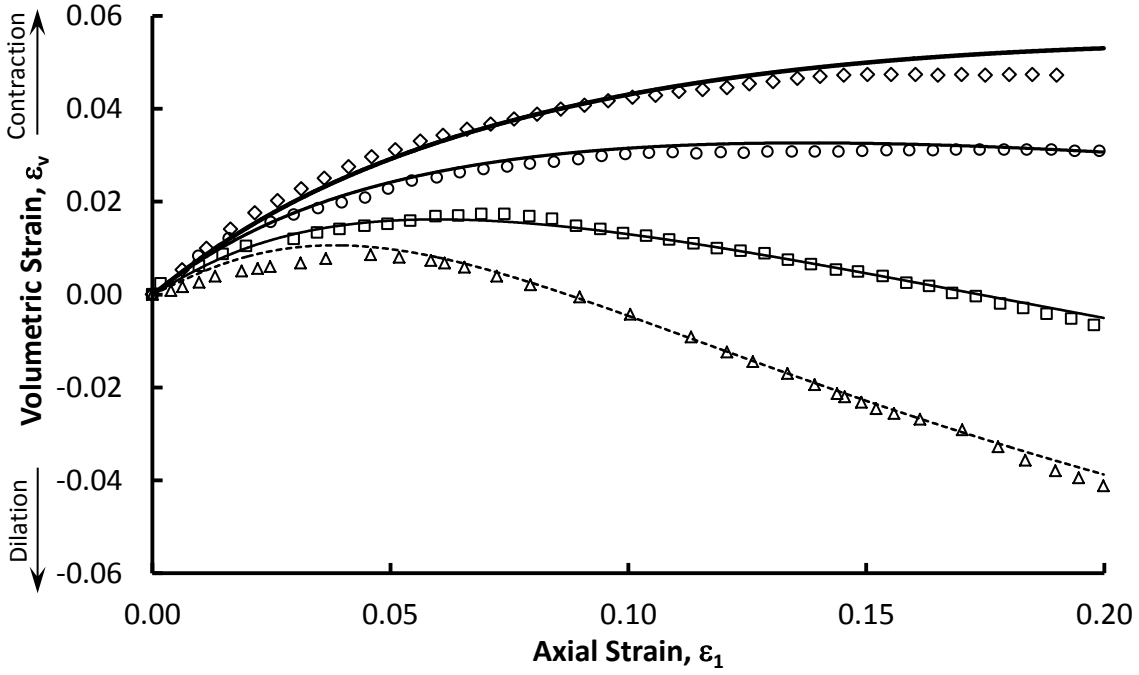

(b)

Figure 10: Triaxial compression tests on crushed ballast (a) $q-\varepsilon_1$ **plot and (b)** $\varepsilon_v-\varepsilon_1$ **plot**

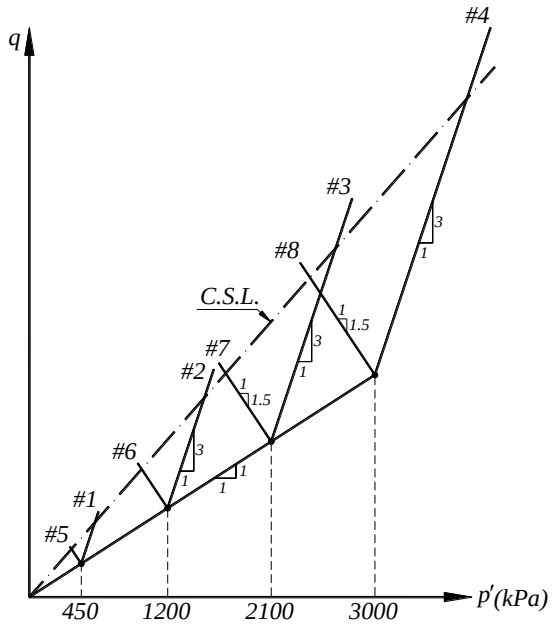

Figure 11: Stress paths used for tests on Nuozadu rockfill (Xiang *et al.*, 2009)

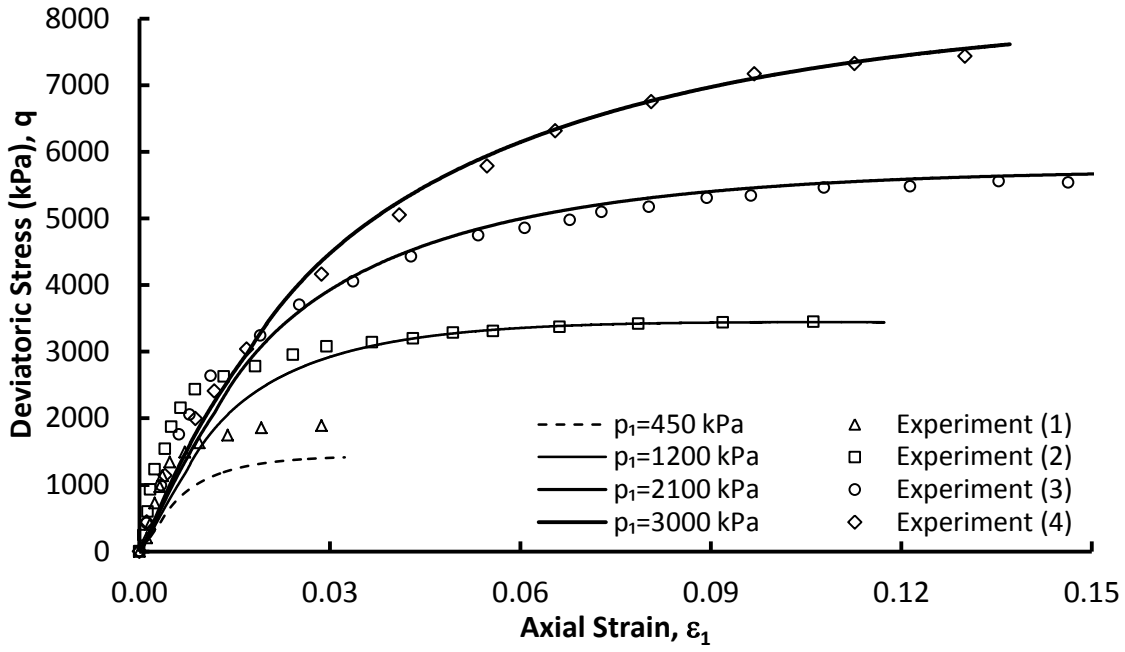

(a)

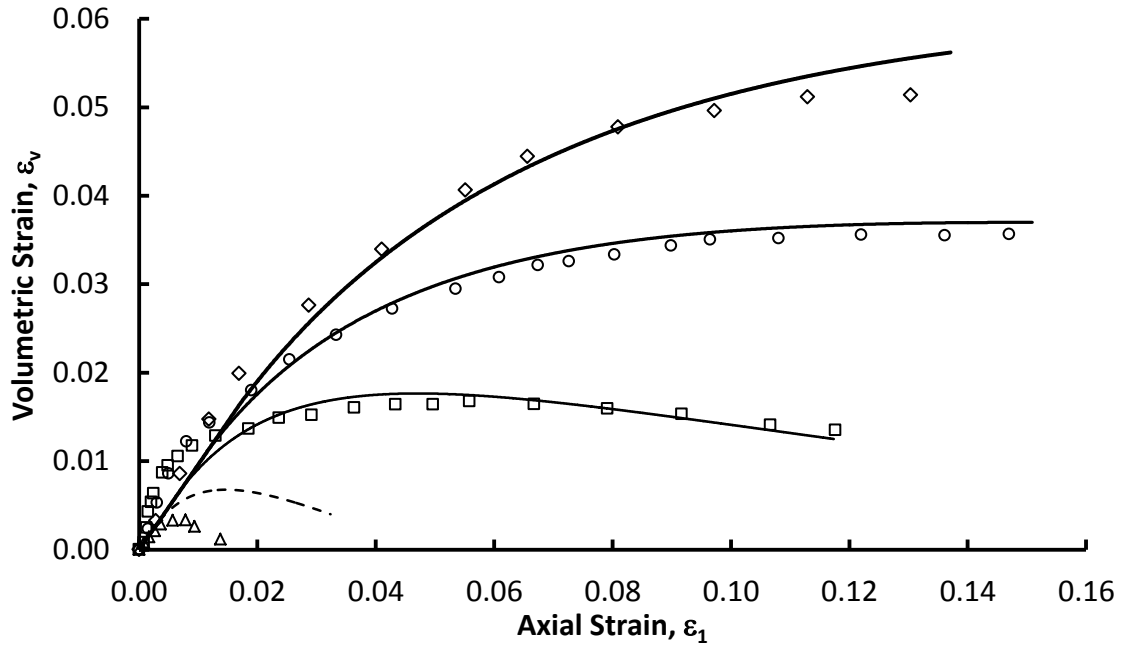

(b)

Figure 12: Triaxial compression tests on Nuozadu rockfill (stress path-1)

(a) $q-\varepsilon_1$ **plot and (b)** $\varepsilon_v-\varepsilon_1$ **plot**

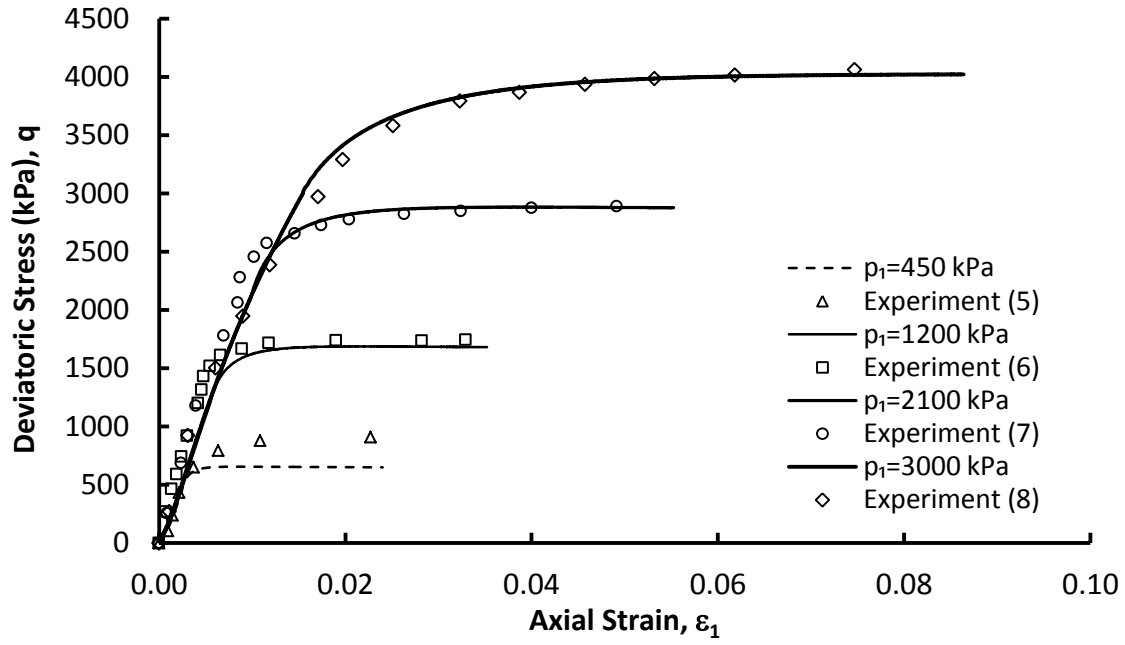

(a)

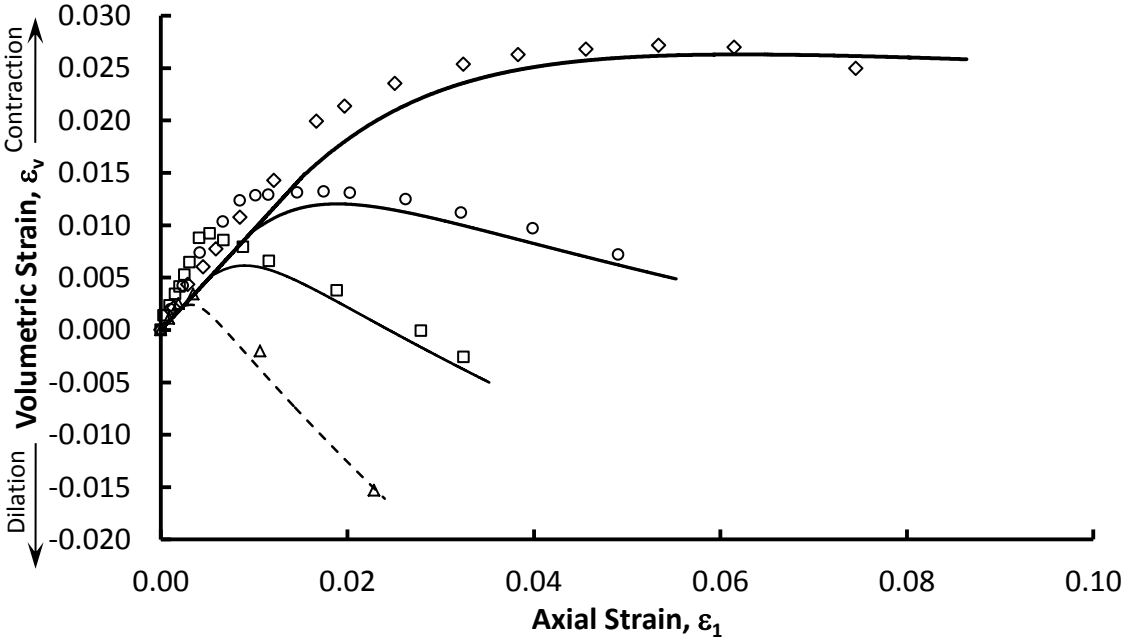

(b)

Figure 13: Triaxial compression tests on Nuozadu rockfill (stress path-2)

(a) $q-\varepsilon_1$ **plot and (b)** $\varepsilon_v-\varepsilon_1$ **plot**

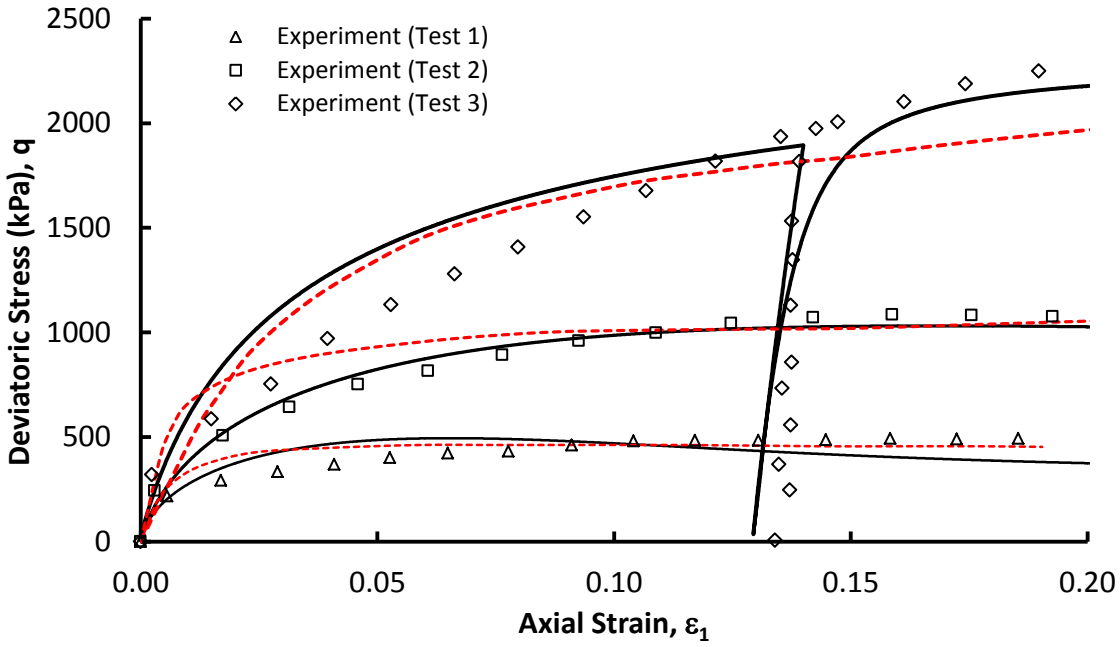

(a)

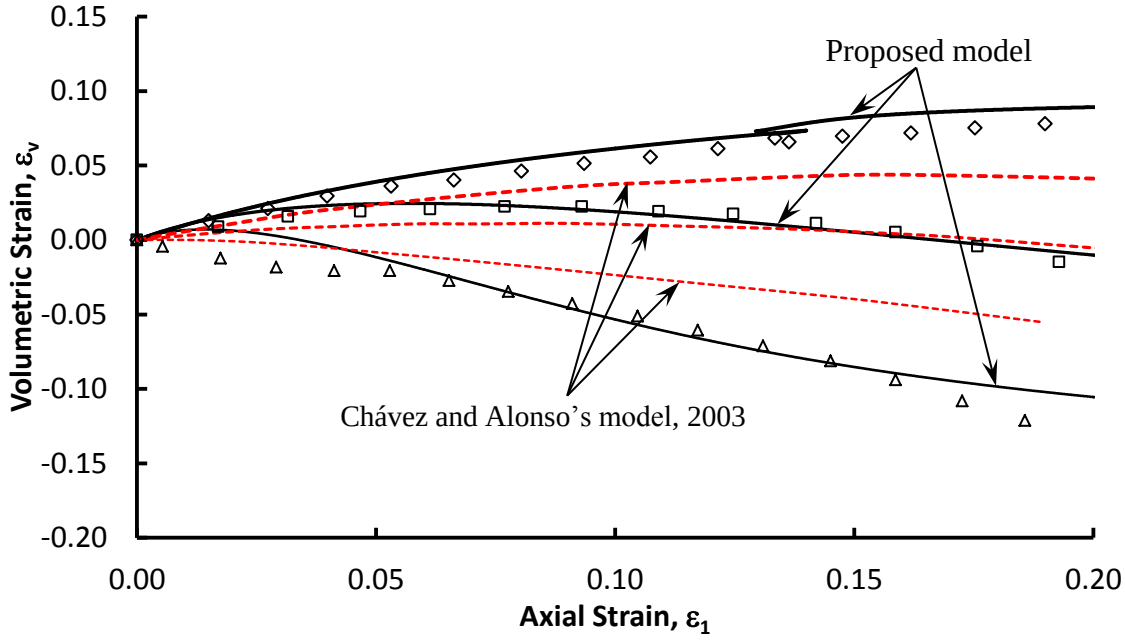

(b)

Figure 14: Triaxial compression monotonic and cyclic tests on crushed Cambric slate (a) $q-\varepsilon_1$ plot and (b) $\varepsilon_v-\varepsilon_1$ plot

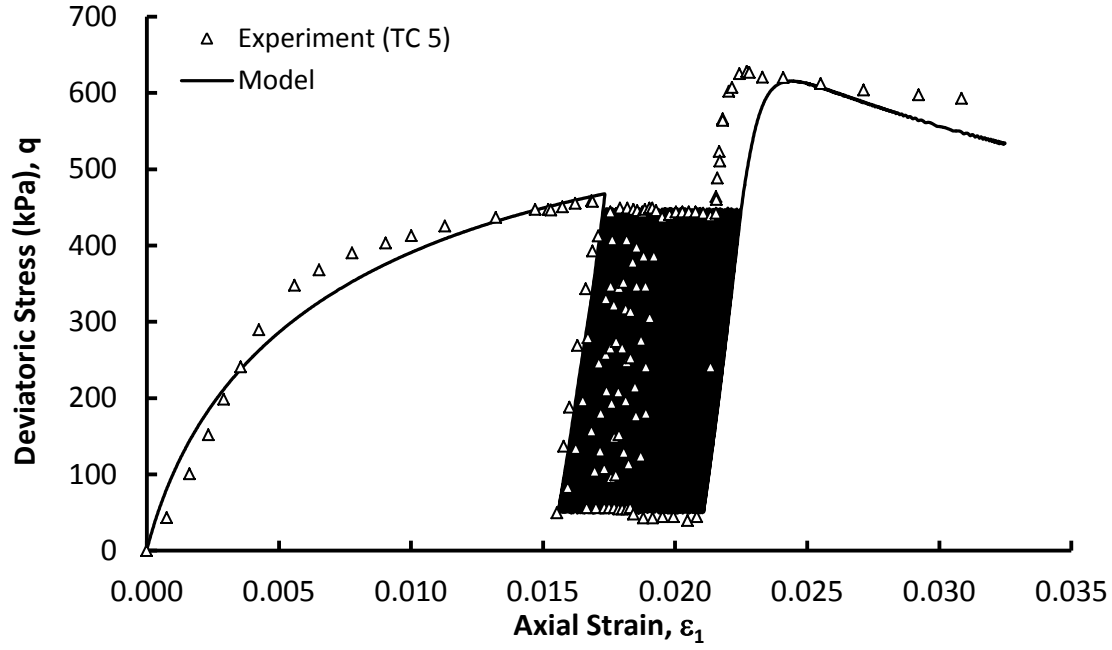

(a)

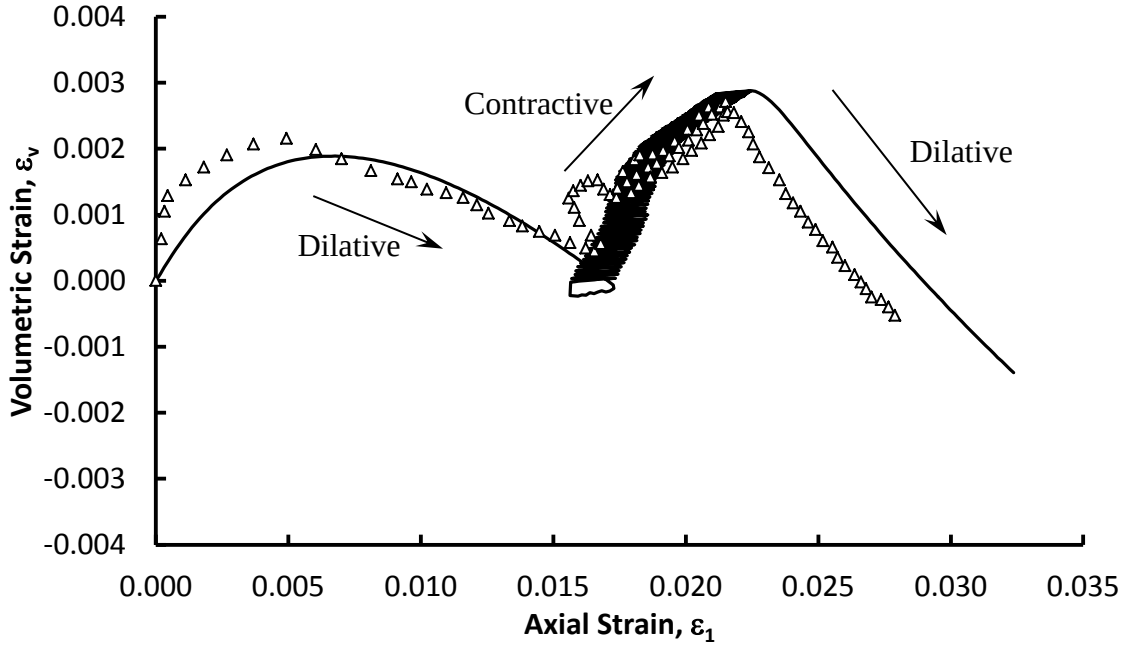

(b)

Figure 15: Triaxial cyclic test on Chiba gravel

(a) $q-\varepsilon_1$ **plot and (b)** $\varepsilon_v-\varepsilon_1$ **plot**

List of Tables

Table 1: Material constants used in simulations for monotonic tests

Parameter Type	Parameter	Ranjit Sagar rockfill	Shah Nehar rockfill	Purulia dam rockfill	Kol dam rockfill	Crushed ballast
Elastic behaviour	p_{ic}	15,000	30,000	20,000	50,000	50,000
	ν	0.29	0.35	0.31	0.32	0.3
Critical state line	υ_l	1.1	1.2	1.2	1.2	1.2
	υ_h	1.433	1.533	1.711	1.711	2.1
	α_1	0.7	0.7	0.5	0.5	0.8
	M_{cs}	2.06	1.4	1.46	1.64	2.0
	p_{cs}	2500	3000	2500	2500	2500
Bounding surface	N	1.5	1.5	1.5	1.5	1.5
	R	3.0	3.0	3.0	3.0	3.0
Particle breakage	α_2	0.3	0.2	0.25	0.25	0.2
	p_r	4000	20,000	5000	5000	10,000
Stress dilatancy	A	0.7	1.0	4.0	1.0	1.0
Hardening	k_{mo}	30.2	33.6	27.3	7.3	1.05
	β_1	1.0	1.0	1.0	1.0	1.0
	β_2	3.1	1.74	3.1	0.3	-0.25

Table 2: Material constants for complex stress paths and cyclic tests

Parameter Type	Parameter	Nuozadu rockfill	Crushed Cambric slate	Chiba gravel
Elastic behaviour	p_{ic}	5×10^6	10,000	50,000
	ν	0.3	0.29	0.3
Critical state line	υ_l	1.26	1.3	1.3
	υ_h	1.84	2.0	2.0
	α_1	0.4	1.8	0.6
	M_{cs}	1.72	1.46	1.55
	p_{cs}	2500	1750	2500
Bounding surface	N	1.5	1.5	1.5
	R	3.0	3.0	3.0
Particle breakage	α_2	0.3	0.4	0.3
	p_r	5000	2000	5000
Stress dilatancy	A	2.0	2.0	1.0
Hardening	k_{mo}	9.45	42.0	34.8
	β_1	1.0	1.0	1.25
	β_2	1.15	1.45	1.0